Ore Geology Reviews 143 (2022) 104763

Contents lists available at ScienceDirect

Ore Geology Reviews

journal homepage: www.elsevier.com/locate/oregeorev

Geology and genesis of the Chomalu polymetallic deposit, NW Iran

Majid Ghasemi Siani [a,*], Behzad Mehrabi [a], Mahya Nazarian [b], Mohammad Lotfi [b], Fernando Corfu [c]

[a] Department of Geochemistry, Faculty of Earth Sciences, Kharazmi University, Tehran, Iran
[b] Research Institute for Earth Science, Geological Survey of Iran, Iran
[c] Department of Geosciences, University of Oslo, Blindern, Oslo N-0316, Norway

ARTICLE INFO

Keywords:
Fluid inclusion
Ore genesis
Intermediate sulfidation
Chomalu deposit
Western Alborz

ABSTRACT

The vein-type Chomalu polymetallic epithermal deposit, located in the Tarom-Hashtjin Metallogenic Province (THMP), western Alborz, formed in two separate mineralized zones controlled by fault zones within andesite and olivine basalt host rocks. The deposit occurs adjacent to the Varmarziar quartz monzonite, quartz monzodiorite, and monzosyenite intrusions. Ore mineralization consists of three stages; (i) an early stage dominated by gold-bearing breccia veins mainly consisting of quartz, pyrite, arsenopyrite, chalcopyrite, minor magnetite and bornite assemblages, (ii) a main stage, which is divided in three sub-stages I, II and III. Sub-stage I is dominated by Pb-Zn-Cu-Ag-rich mineral assemblages including galena, Fe-poor sphalerite, minor chalcopyrite, tetrahedrite, and pyrite. Sub-stage II is only represented by galena and Fe-poor sphalerite. Sub-stage III is defined by Fe-Mn-Zn-Ca-Mg carbonate minerals. The late supergene stage (iii) is characterized by malachite, covellite, chalcocite, cerussite, and Fe-oxide and hydroxides. Microthermometry of primary fluid inclusion assemblages indicate homogenization temperatures (Th) of 253° to 305 °C and salinities of 3.5–4.82 wt% NaCl equivalent in the early stage. The main stage indicates homogenization temperatures (Th) of 200° to 280 °C and 180° to 235 °C with salinities of 2.18–4.96 and 0.53–2.90 wt% NaCl equivalent for the sub-stages I and II, respectively. Ore precipitation was possibly caused by simultaneous dilution and cooling of hydrothermal fluids. The epithermal mineralization in the Chomalu deposit may be classified as an E-type intermediate sulfidation epithermal deposit in the extensional back-arc regime.

1. Introduction

Porphyry-epithermal systems are important sources of base and precious metals (Sillitoe and Hedenquist, 2003; Sillitoe, 2010). They are subdivided into two main groups, namely deep porphyry copper systems, transitional into shallower porphyry-related base-metal vein and replacement deposits (Henley and Adams, 1992; Hemley and Hunt, 1992; Einaudi et al., 2003; Baumgartner et al., 2008; Sillitoe, 2010; Catchpole et al., 2012), and ultimately near the surface termed high, intermediate, and low-sulfidation epithermal deposits (HS, IS, and LS) (Hedenquist et al., 1998; Muntean and Einaudi, 2001; Einaudi et al., 2003; Wang et al., 2019). The Mesozoic to Cenozoic Alpine-Himalayan Orogenic Belt (Tethyan orogenic belt, TOB), stretching from the Alps, through the Balkan Peninsula, Turkey, Iran, Pakistan, Tibet, Indochina and ultimately into the southwest Pacific, has the best-known concentration of epithermal-porphyry systems (Blundell et al., 2005; Schettino and Turco, 2011; Richards, 2015). Located in the middle of this extensive TOB, Iran hosts many porphyry-epithermal ore mineralized systems along (i) the NW-SE trending Urumieh-Dokhtar Magmatic Arc (UDMA) (e.g., Richards, 2015 and references therein), (ii) the E-W trending Alborz Magmatic Arc (AMA) (Shamanian et al., 2004; Mehrabi and Siani, 2012; Tale Fazel et al., 2019), and (iii) the East Iran Magmatic Assemblage (Richards et al., 2012 and references therein). The western Alborz, here known as the Alborz-Azerbaijan Magmatic Belt, is subdivided into the northwestern Ahar-Arasbaran Belt (AAB) and the southeastern Tarom-Hashtjin Metallogenic Province (THMP) (Ghasemi Siani et al., 2015; Fig. 1).

The THMP is one of the most important epithermal provinces in Iran (Ghasemi Siani et al., 2020 and references therein). The Chomalu epithermal polymetallic deposit is located in 70 km north of Zanjan province in the THMP. Ancient workings and dumps were found at several locations near hydrothermal vein occurrences. A new exploration

* Corresponding author.
E-mail address: m.ghasemi@khu.ac.ir (M. Ghasemi Siani).

https://doi.org/10.1016/j.oregeorev.2022.104763
Received 17 September 2021; Received in revised form 29 January 2022; Accepted 8 February 2022
Available online 16 February 2022

program in the Chomalu deposit conducted by the Karend Sadr Jahan Company in Iran with 27 boreholes (totally 4500 m) and 12 trenches (totally 110 m), indicates 0.2 Mt of Pb-Zn-Cu-Au-Ag ore with an average grade of 4.7% Pb, 3.2% Zn, 0.5% Cu, 1.08 g/t Au, and 60 g/t Ag.

In this paper, we first summarize the main aspects of mineralogy, mineral chemistry, and fluid inclusions of the mineralized veins, then address some of the key questions related to the evolution of the hydrothermal system, mechanisms of ore deposition and genesis of the Chomalu epithermal deposit. Finally, we compare it with the Cordilleran-type, base-metal veins, and present an overview of tectono-magmatic setting in the western Alborz and associated porphyry-epithermal ore mineralization. Results of this study, combined with published literature on other ore deposits in the THMP (especially Glojeh deposit), are used to define a framework for exploration of the epithermal base-metal veins in the THMP and possibly discovery of buried porphyry ore systems.

2. Regional geology

The Cenozoic Alborz Magmatic Arc (AMA) in the northern part of Iran consists of Eocene to Miocene porphyritic and non-porphyritic, massive lava flows of andesite, basaltic andesite, basalt, and sedimentary rocks composed of both marine and subaerial sequences underlain by the Precambrian metamorphic basement, associated with plutonic intrusions, followed by the Cambrian and Permian metamorphic and Mesozoic sedimentary rocks (mainly limestone and sandstone) (Azizi and Jahangiri, 2008).

The stratigraphy of the THMP is dominated by Eocene mafic to acidic volcanic rocks and Eocene intrusions overlain by Oligo-Miocene volcano-plutonic and sedimentary rocks (siltstone, sandstone, limestone and etc.). This tectono-magmatic metallogenic region is characterized by numerous epithermal ore systems (Fig. 2). The main epithermal ore mineralization are; Chodarchay HS deposit (0.5 Mt; 0.9% Cu and 2 g/t Au; Yasami et al., 2017), Glojeh HS to IS deposit (2.3 Mt of 3% Pb, 2.2% Zn, 1.5% Cu, 2.9 g/t Au, and 350 g/t Ag; Mehrabi et al., 2010, 2016), Khalifehlou HS deposit (60,000 t; 8% Cu, 6 g/t Au, and 7 g/t Ag; Esmaeli et al., 2015), Aliabad-Khanchy IS deposit (0.2 Mt with 1.3% Cu; Kouhestani et al., 2018), Shah-Ali-Beiglou IS deposit (3% Zn, 7% Pb, 1.1% Cu, and 24 g/t Ag; Mikaeili et al., 2018), Lohneh IS deposit (Zamanian et al., 2016), Nikuyeh LS deposit (Aghajani et al., 2016), Chargar (Mousavi Motlagh and Ghaderi, 2019), and Aqkand LS deposit (Kouhestani et al., 2017). The highly altered Eocene volcanic rocks are the main host rocks of the epithermal ore deposits and mineralization, which are dominantly controlled by the NNE- and NE- and NNW- and NW-trending faults (Ghasemi Siani and Lentz, 2022).

The Chomalu epithermal deposit is located in the THMP, close to the well-studied Glojeh epithermal ore deposit. The latter consists of two separately mineralized polymetallic veins, namely North Glojeh and South Glojeh (cf. Mehrabi et al., 2016; Fig. 3). The Eocene-Oligocene volcanic and volcaniclastic rocks are widespread in this region, mainly including well layered and dark colored lithic and vitric tuffs, basic tuff with interlayered trachybasalt, trachyandesitic basalt and minor andesitic basalt and rhyolite to rhyodacite. The volcanic rocks are intruded by two granitoid stocks, namely Goljin and Varmarziar intrusions (Ghasemi Siani et al., 2015). Several subvolcanic dikes, characterized by quartz, biotite, and plagioclase phenocrysts, intruded the lithic tuff unit.

3. Sampling and analytical methods

About 160 surface and drill core samples were collected from mineralized veins and alteration zones during field work. One hundred

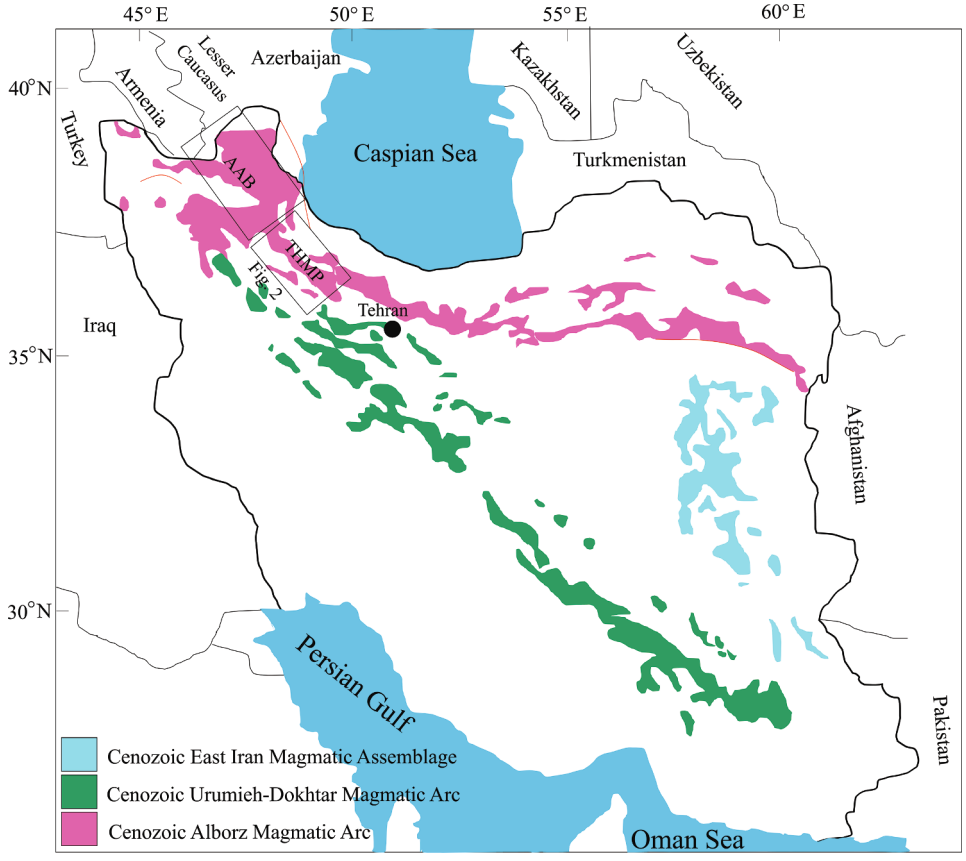

Fig. 1. Simplified geology map of Iran and location of the Tarom-Hashtjin metallogenic province (THMP) in the south and Ahar-Arasbaran Belt (AAB) in the north in the western Alborz Magmatic Arc (Ghasemi Siani et al., 2020).

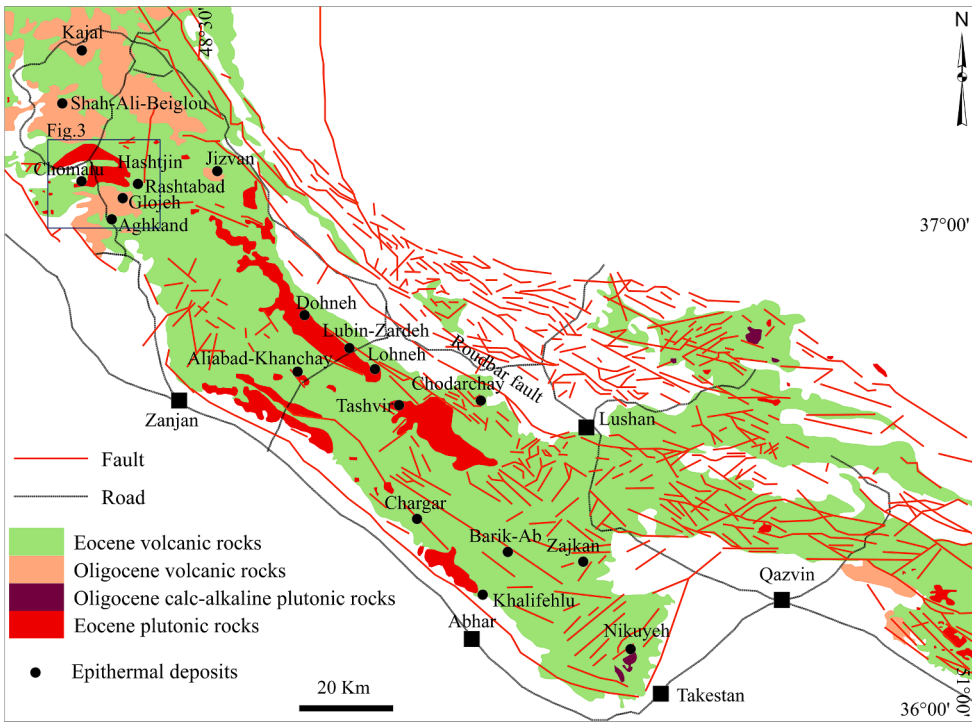

Fig. 2. Simplified geological map of the THMP (Ghasemi Siani and Lentz, 2021) and location of some major epithermal-porphyry ore deposits.

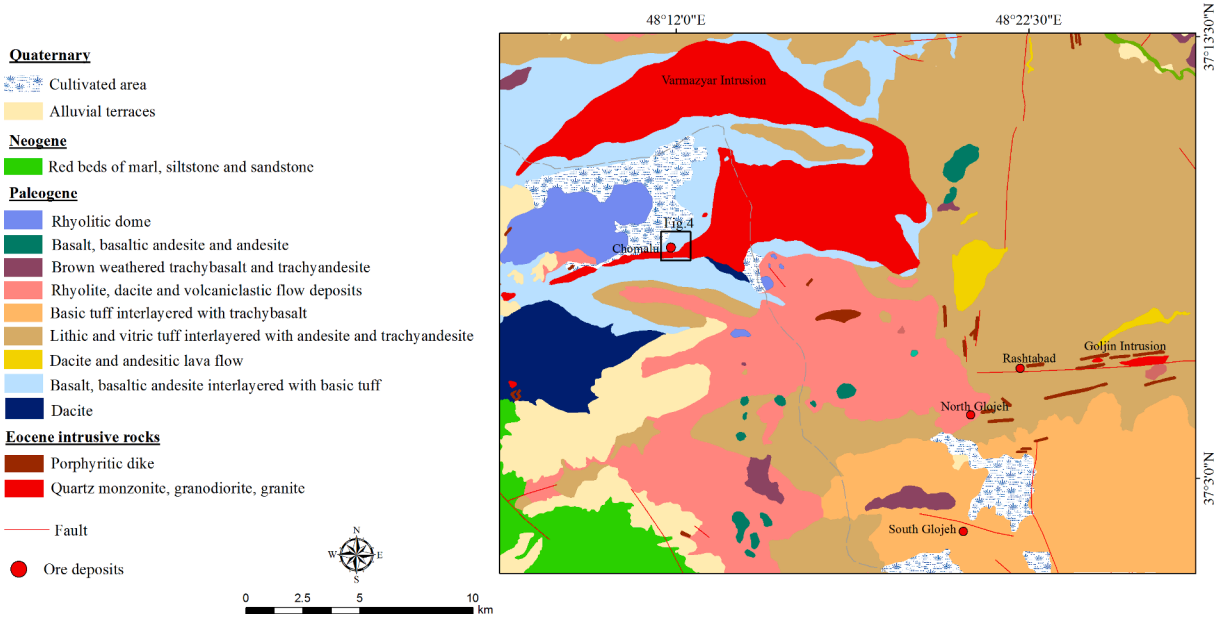

Fig. 3. Simplified geology map of the Chomalu and Glojeh epithermal ore deposits (modified after Hashtjin 1/100000 quadrangle map; Faridi and Anvari, 2005).

and twelve polished thin sections were prepared and their textures and mineralogy studied by optical microscopy. Optical microscopy were carried out at the Iranian Mineral Processing Research Center (IMPRC) and Kharazmi University of Tehran using an Axioplan2 Zeiss reflected-transmitted research microscope. In addition, selected polished samples were examined by scanning electron microscope (SEM), using energy dispersive spectroscopy (EDS) analysis for mineral identification and later quantitative analysis by electronic probe microanalysis (EPMA).

SEM studies were carried out by a Zeiss Evo model at Kharazmi University. The SEM-EDS analyses and secondary electron (SEM-SE) images were acquired using beam currents of 0.05 and 5nA and an electron acceleration voltage of 5 to 20 kV. The EPMA analyses were carried out using a Cameca SX100 instrument mounted with five WDX spectrometers at IMPRC using an accelerating voltage of 15 kV and 15nA current for silicates. The detection limit is ~100 ppm for all elements.

Fifteen powder samples from alteration zones and supergene ore were studied by the XRD method after grinding in an agate mortar and pestle down to <60 μm diameter. The XRD analyses were performed using a Philips (Xpert-Pro model) instrument with CoKα1 (1.789A°) primary beam, mono-chromator on secondary optics, 40 kV power and 35 mA current at the IMPRC. The mineralogical composition of the

samples was determined using quantitative XRD analysis (Rietveld method). Data were collected from 4.0 to 80.0° 2θ, with a step size of 0.02°.

Fifteen doubly polished sections of quartz, fluorite, and sphalerite from mineralized veins were prepared for fluid inclusion microthermometry using a Linkam THMS 600 freezing-heating stage, mounted on a ZEISS Axioplan2 research microscope at IMPRC. The precision of the temperature measurements was less than ± 1 °C for heating and ± 0.3 °C for freezing.

4. Mineralization style and hydrothermal alteration

The exposed strata are mainly andesitic basalt, andesite, trachyandesite, and olivine basalt, with minor rhyolite to dacite, intruded by quartz monzonite, porphyritic quartz monzodiorite, and monzosyenite (Fig. 4a). The ore bodies are structurally controlled by NNW- to NNE-trending systems (Fig. 5a), and subdivided in two zones; consisting of several mineralized veins (Fig. 4b). The first mineralized zone is located in the andesitic host rocks close to the quartz monzonite intrusion (Fig. 5a). It is composed of five main E-W-trending polymetallic veins (I, II, III, IV and V) and several accessory veins, in association with hydrothermal breccias and silica-carbonate open space fillings (Fig. 5b, c). Total length of the veins is 800 m with 2 to 20 m width (average of 6 m). They developed directly on the main fault, N70E with dip 75–80° to the SE, and experienced cataclastic deformation due to post mineralization fault reactivation. Silicification is the main alteration in these ore vein systems, surrounded by sericitic alteration.

The second mineralized zone, located farther north (Fig. 4b), contains of five ore veins, namely, V1, V2, V3, V4 and V5, mostly hosted by the olivine basalts. These veins, with a total length of 950 m and 4 m width in average, are orientated NNW (N10-35 W) with a dip of 60–70° NE. They are characterized by base-metal mineralization with intensively silicic, sericitic, argillic and propylitic alteration zones.

A variety of primary ore textures has been identified, including veins, veinlets, massive, crustiform banding, colloform, hydrothermal breccia, stockwork, and disseminated textures (Fig. 5d–f). The first mineralized zone is Cu-Au rich, whereas the second mineralized zone is rich in Ag-Pb-Zn. It is evident that from east to west, in the first mineralized zone and south to north in the second mineralized zone, there is an increasing order of Zn > Pb + Ag > Cu + Au content. Ore minerals in both ore bodies are dominated by pyrite, chalcopyrite, arsenopyrite, magnetite, sphalerite, galena and tetrahedrite, siderite, smithsonite, rhodochrosite, magnesite, oligonite, hemimorphite, chalcocite, cerussite, covellite, malachite, hematite, and goethite. Quartz, fluorite, and calcite are the main gangue minerals.

Hydrothermal alteration in the mining area is intense and developed as envelopes around the veins in a range of one to tens of meters, consisting of silicification and argillization, followed by sericitization and propylitization. Silicification is the main alteration and is characterized by massive and vuggy silica, quartz, chalcedony and anatase associated with disseminated pyrite (Fig. 6ai, aii). Vuggy quartz is more common with Au-Cu mineralization in the first mineralized zone, whereas massive quartz is dominant with galena and sphalerite veins. Sericitization is less intense and represented by sericite, quartz, pyrite, arsenopyrite, and minor calcite in which plagioclase phenocrysts are partly replaced by sericite (Fig. 6bi, bii). Argillic alteration is well-developed around the base-metal veins and mainly characterized by quartz, kaolinite, and illite, and less common montmorillonite, chlorite, and pyrite, with plagioclase and K-feldspar replaced completely by kaolinite and illite (Fig. 6ci, cii). Propylitic alteration in the outer alteration zone consists of calcite, epidote, chlorite, and albite (Fig. 6di, dii). Farther out at the regional scale, beyond the mineralized zones of the Chomalu ore mining district, supergene alteration includes widespread acid-sulfate supergene alunite, jarosite, and gypsum.

5. Paragenetic succession and mineral chemistry

Although the mineral assemblages are similar in both ore bodies,

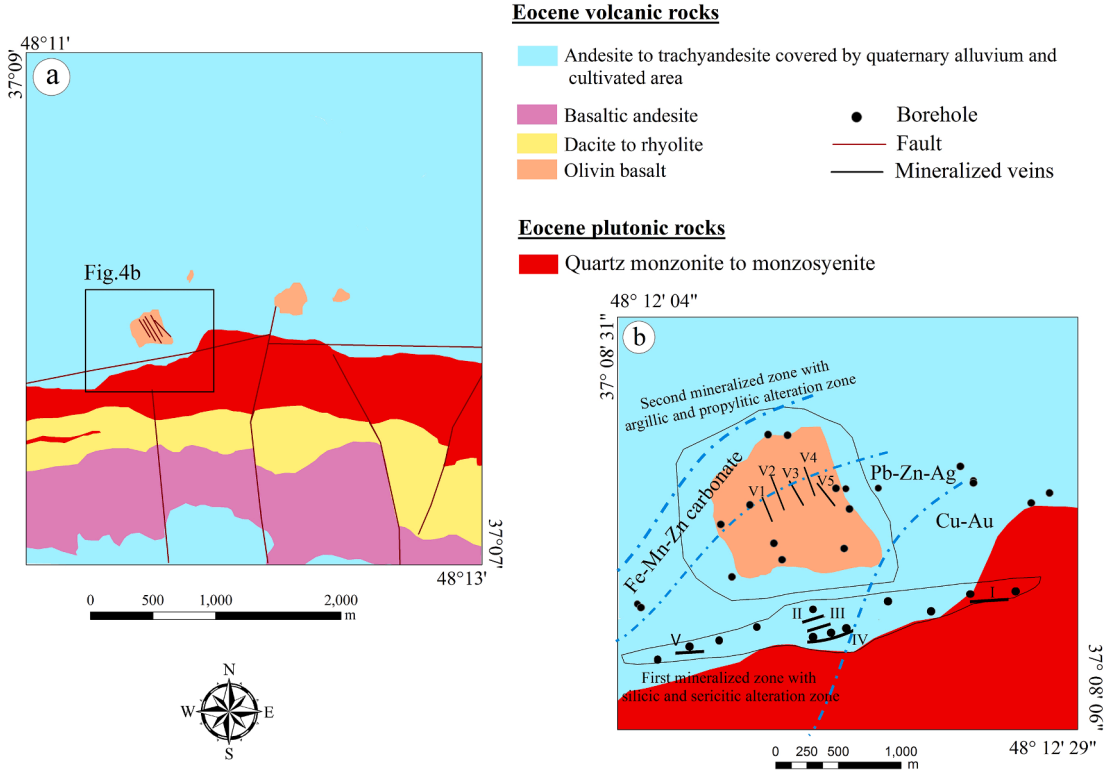

Fig. 4. a) Tectonic-petrological geological map of the Chomalu deposit at 1/5000 scale, b) Geological map of the structure, mineralized vein, alteration zones, and petrological settings of the Chomalu ore veins at 1/1000 scale.

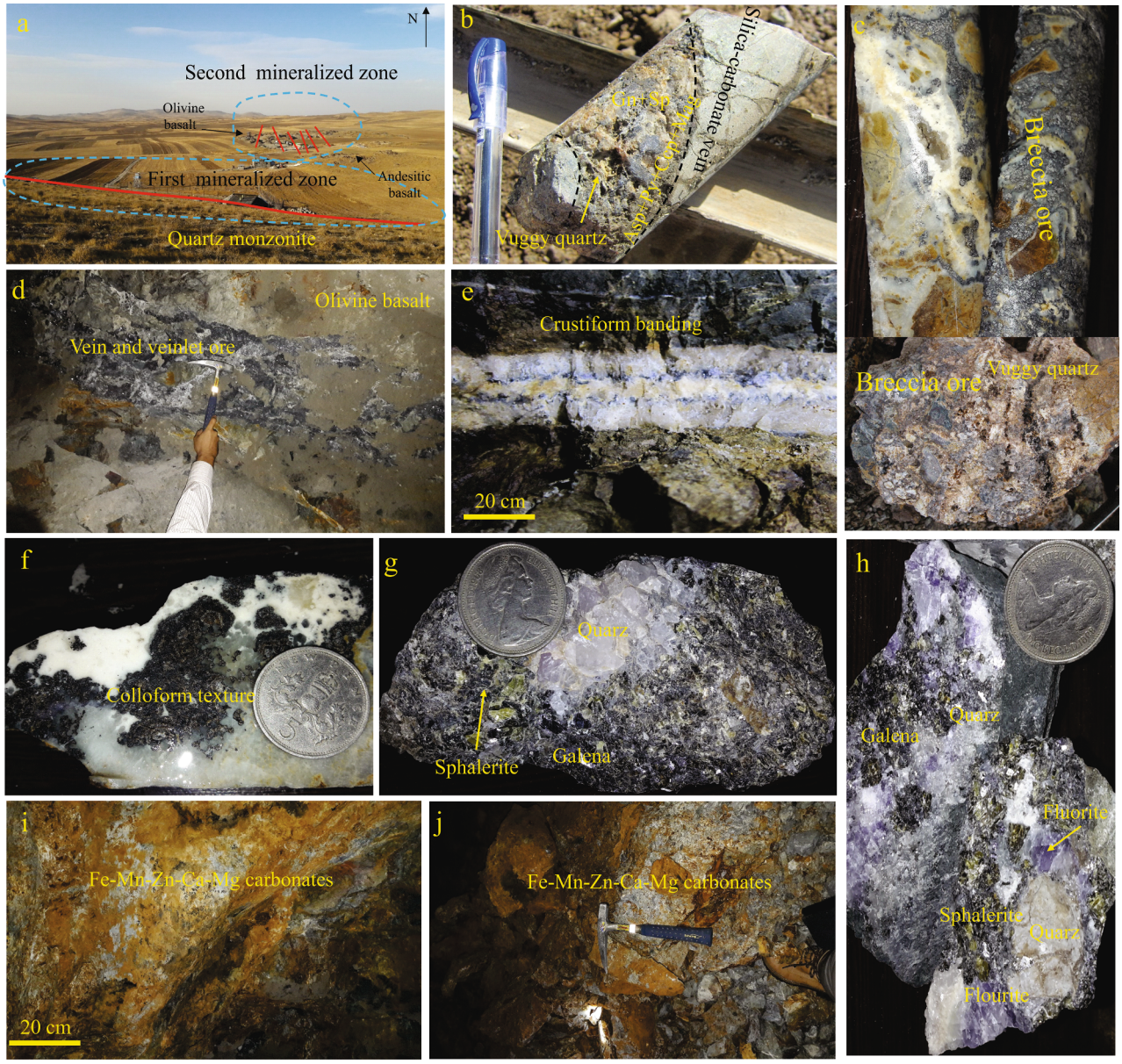

Fig. 5. Outcrop, hand specimen and borehole cores of mineralization zones: a) General view of the Chomalu deposit with an E-W fault controlling the first mineralization zone close to quartz monzonite intrusive rocks and several NNW-trending fault associated with the second mineralization zone; b) Silica-carbonate vein with vuggy texture quartz, containing early Asp + Py + Ccp + Mag and late Gn + Sp mineralization; c) Hydrothermal breccia vein associated with vuggy texture (below) comprising fragments of quartz and wall rock cemented by base-metal mineralization; d) Vein and veinlet texture of the main stage of mineralization; e) Crustiform banding comprising of coarse-grained quartz and fluorite with base metal, the main stage of mineralization, f) Colloform texture ore; g) Massive ores containing coarse-grain galena and sphalerite with abounding of tetrahedrite inclusion with coarse-grained quartz in the sub-stage I, h) Sphalerite-galena zone with violet coarse-grained fluorite and milky quartz in the sub-stage II, i and j) Fe-Mn-Zn-Ca-Mg carbonates assemblages in the sub-stages III of the main stage of mineralization. Abbreviations: Py, pyrite; Asp, arsenopyrite; Ccp, chalcopyrite; Gn, galena; Sp, sphalerite, Mag, magnetite.

there is a weak zonation in the base-metal assemblages (Fig. 4b). The internal part contains pyrite, chalcopyrite, and magnetite with minor bornite, whereas the external part contains more sphalerite, galena, quartz, and fluorite. Fig. 7 shows a paragenetic sequence of ore and gangue minerals in the Chomalu ore deposit.

According to field observations, cross-cutting relationships and mineral assemblages, the ore-forming processes can be subdivided into three stages: 1) an early Cu-Au-As-Fe stage, 2) the main ore stage divided into Pb-Zn-Cu-Ag-rich minerals (I), Pb-Zn-rich minerals (II) and late Fe-Mn-Zn-Ca-Mg carbonates (III), and finally 3) late supergene weathering stage. The early stage is characterized by vuggy quartz and silica-carbonate veins containing disseminated pyrite, arsenopyrite, chalcopyrite, bornite, and magnetite (Fig. 8a). Magnetite formed as anhedral and locally subhedral crystals and contains pyrite inclusions, with an almost homogeneous composition. Pyrite occurs as euhedral to anhedral, massive and disseminated crystals, and shows late overgrowths with arsenian pyrite (Fig. 8b). Three points analyses of pyrite indicate that its composition is almost constant, with 46.31% to 46.57 wt% Fe and traces of arsenic (0.02 to 0.15 wt%) (Table 1). Overgrowths on pyrite have more arsenic (up to 0.45 wt%) and gold content in pyrite is low (0.01 wt%). We cannot identify the host minerals for gold mineralization, although results of chemical analysis indicate that some samples from these veins have up to 3 ppm (g/t) Au. Chalcopyrite and minor bornite usually occur in association with pyrite and replace the pyrite along fractures, indicating a later formation. Chalcopyrite contains 0.01–0.04 wt% As. Quartz and calcite are the main gangue

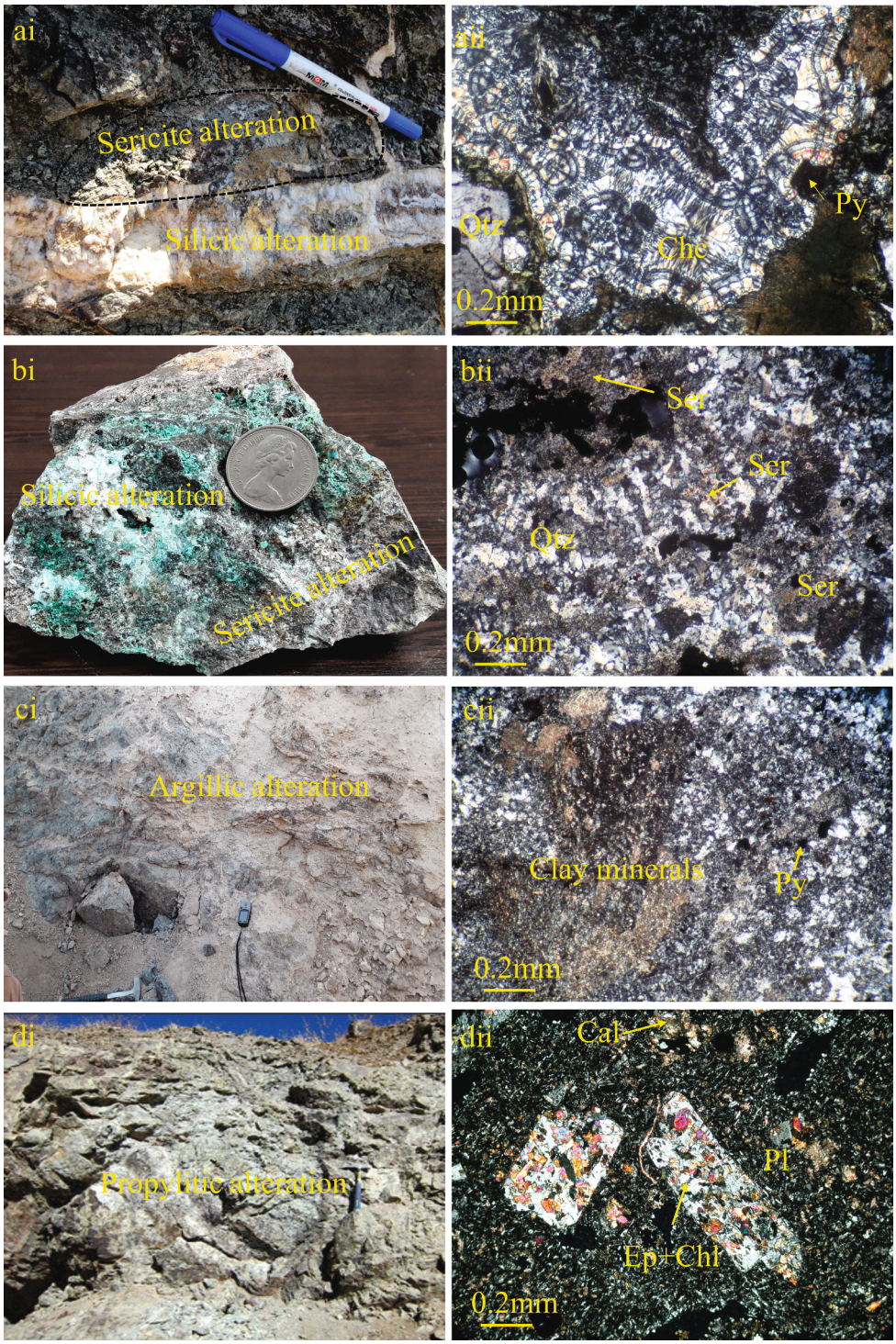

Fig. 6. Filed and photomicrograph of the main alteration zones related to the ore mineralization. a) ai, silicic vein containing quartz and chalcedony filling the pores of volcanic rocks associated with pyrite (aii); b) bi, andesitic rock with intensively sericite and silicic alterations associated with quartz, white mica (sericite) and pyrite as the main alteration mineral (bii); c) ci, widespread argillic alteration around the base metal ore indicating that plagioclase crystals completely replaced by clay minerals, such as kaolinite, illite, and montmorillonite (cii), d) di and dii show propylitic alteration in olivine basalt and andesitic rocks in which plagioclase crystals partially replaced by epidote and chlorite. Abbreviations: Py, pyrite; Chc, chalcedony; Qtz, quartz; Ser, sericite; Ep, epidote; and Chl, chlorite.

minerals of this stage.

The main ore-stage zones show a well-developed lateral and vertical zoning. Quartz and fluorite are major gangue minerals in the main stage. Three episodes of quartz deposition are recognized including crustiform and massive quartz, massive quartz-fluorite, and vein/veinlets containing base-metal sulfides and then barren fine smoky quartz vein.

The most internal part (I) consists of veinlets and massive ore of galena, sphalerite, chalcopyrite, pyrite, and tetrahedrite, associated with Ag-bearing minerals, and with kaolinite and illite alteration minerals; termed as the Pb-Zn-Cu-Ag zone (Fig. 5g). Sub-stage I is characterized by deposition of coarse-grained quartz, galena, and sphalerite in form of massive, veins and veinlets. Galena and sphalerite are main minerals formed as intergrowths though some inclusion of galena observed in sphalerite and vice versa (Fig. 8c, Fig. 9a). Ag-bearing tetrahedrite inclusions are abundant in both galena and sphalerite (Fig. 8d, Fig. 9b), and there are also chalcopyrite inclusions in tetrahedrite, galena, and sphalerite (Fig. 8e, Fig. 9c). Pyrite also occurs a inclusions in sphalerite (Fig. 9d). These observations indicate that ore assemblages formed simultaneously. We cannot detect any silver minerals by EPMA and just covellite in the late supergene stage formed around galena contains up to 5 wt% Ag (Table 1). The iron and cadmium contents of sphalerite are generally low (0.12–0.92 wt% and 0.01–1.97

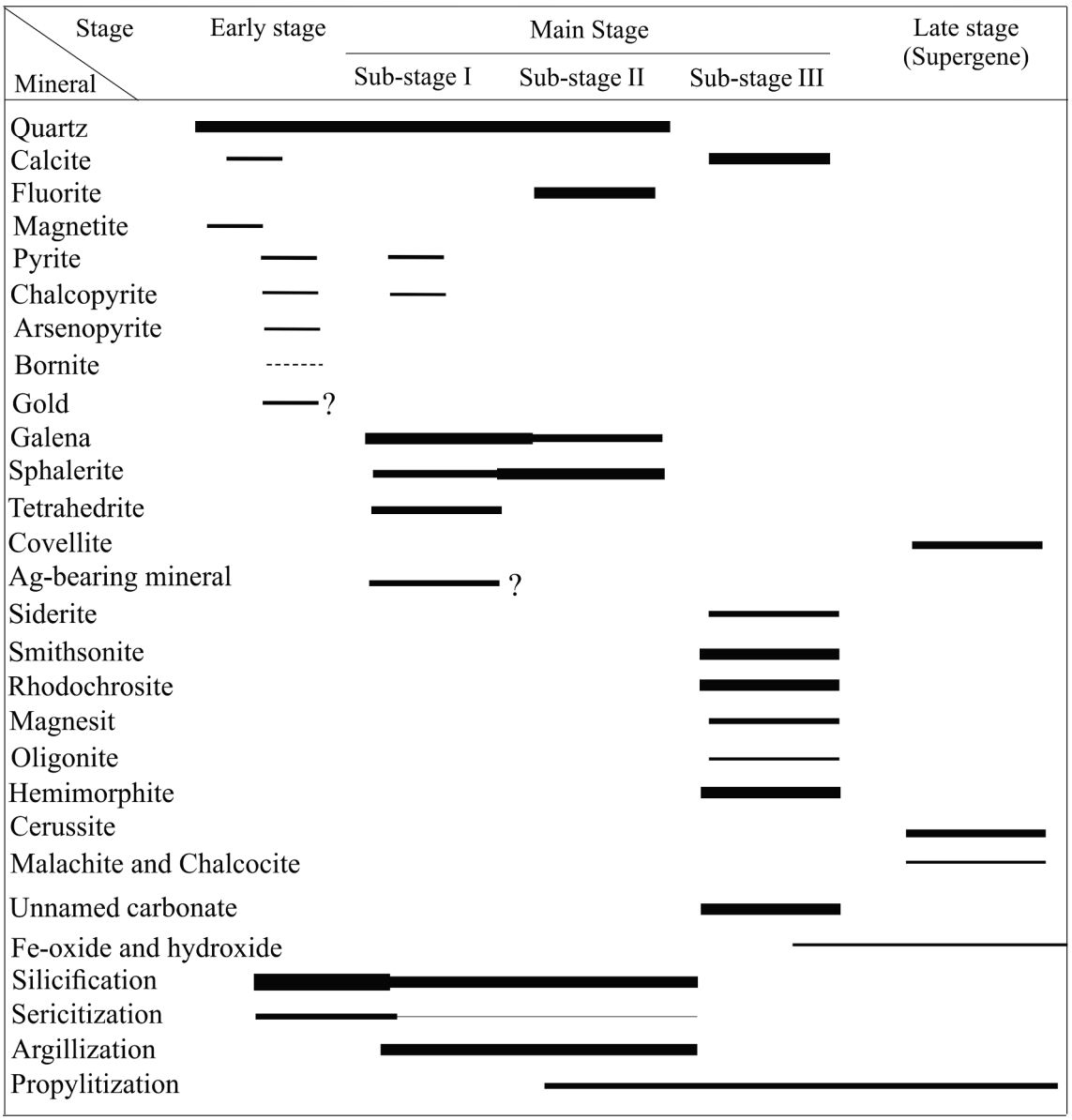

Fig. 7. Ore and gangue minerals depositional sequence associated with the main alteration zone at the Chomalu deposit. Thicknesses of lines show frequency of minerals. Stages of mineralization are described in the text.

wt%, respectively). Chalcopyrite inclusions in galena and sphalerite are close to stoichiometric chemical compositions. Due to supergene alteration cerussite formed in galena rims. Since the Cu content in the galena are noticeable and inclusions of Ag-bearing minerals, like tetrahedrite presence in the galena, Ag-rich covellite (up to 5 wt% Ag), and Ag-bearing cerussite (up to 2 wt% Ag) formed within the galena (Fig. 8f, Fig. 9e). These supergene alterations locally reach down to a depth of 70 m below the surface, and produced Ag- and Pb-rich oxidized ores around sub-stages I and II. Galena tends to contain 0.02 to 0.08 wt% As, 0.01 to 0.34 wt% Bi, below detection limit to 0.55 wt% Cd, 0.01 to 0.09 wt% Ag, and 0.15 to 8.99 wt% Cu. The tetrahedrite is rich in copper (averages 36.86 wt%) and zinc (6.85 to 7.49 wt%) with Ag contents of 0.47 to 2.37 wt%.

Zone I is succeeded outward to zone (II), which is massive to crustiform ores containing galena and sphalerite without tetrahedrite and Ag-bearing minerals, referred as the sphalerite-galena zone (Fig. 5h). Sub-stage II is characterized by massive and open space filling textures in association with medium- to coarse-grained quartz and fluorite, and coarse-grained sphalerite and galena (Fig. 8g and h). Iron content in sphalerite is low (0.41 to 0.83 wt%). The composition of galena is close to stoichiometric (Bi content is 0.31 to 0.63 wt% and Te content is 0.01 to 0.12 wt%).

Zone (III) includes Zn-Mn-Fe-bearing carbonates, referred as Zn-bearing carbonate zone, depicted as a relatively homogeneous thin halo which almost completely surrounding the sphalerite-galena zone (Fig. 5I and j). In contrast to the other zones, sub-stage (III) is virtually devoid of sulfides, consisting siderite, smithsonite, rhodochrosite, magnesite, oligonite, and hemimorphite (Fig. 8i, Fig. 9f) and some unnamed carbonate as well. They occur in patches and massive zones, <15 m long and 2 m thick, with grades commonly in the range of 1 to 4 wt% Zn.

There is no sharp boundary between sub-stages I and II. Some samples display galena and sphalerite zone accompanied by Pb-Zn-Cu-Ag, suggesting that the transition between these sub-stages of main ore stage was gradual. On the other hand, there is a sharp boundary between sulfide zones (Sub-stages I and II) and non-sulfide zones (III). The increasing abundance of sphalerite relative to galena with increasing distance from the Cu-bearing zones is a remarkable feature of the main

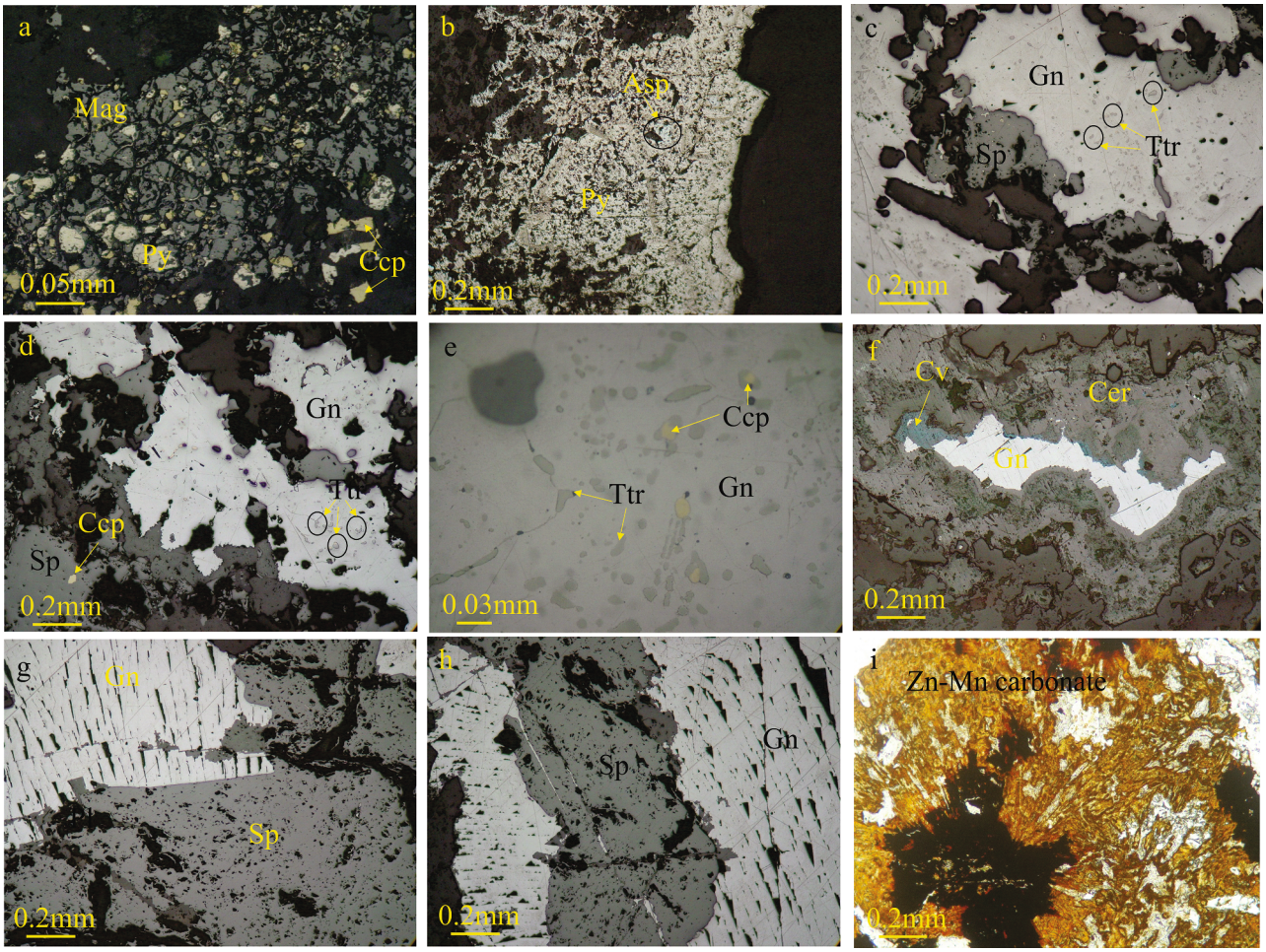

Fig. 8. Reflected light microscope photomicrographs of the Chomalua ore minerals (except i, transmitted light photomicrographs) in cross polars: a) Euhedral to subhedral magnetite surrounded by chalcopyrite and pyrite of the early stage; b) Late overgrowth of pyrite with more As content and inclusion of arsenopyrite in pyrite; c and d) Galena and sphalerite with tetrahedrite inclusion of the sub-stage I; e) Abundant tetrahedrite inclusions in galena and chalcopyrite inclusion in tetrahedrite of the sub-stage I; f) Galena with cerussite rims formed by supergene oxidation; g and h) Coarse-grained galena and Fe-poor sphalerite intergrown with gangue minerals (quartz and fluorite) of the sub-stage II, and i) Zn-Mn-Mg carbonate mainly containing smithsonite and rhodochrosite of the sub-stage III. Abbreviations: Py, pyrite; Asp, arsenopyrite; Ccp, chalcopyrite; Gn, galena; Sp, sphalerite, Mag, magnetite; Cv, covellite; Mal, malachite; Cer, cerussite; Ttr, tetrahedrite.

ore stage. In general, in parts of the main ore stage galena predominates over sphalerite, which is also distinguished by up to 150 g/t Ag; we presume that, except for tetrahedrite inclusions, there may be fine-grained Ag-bearing minerals as inclusions of the main silver sulfides (likely argentite and acanthite) in galena.

6. Fluid inclusions

Fluid inclusion assemblages (FIAs) have been studied in quartz from the early stage (Qtz1), main stage including sub-stage I (Qtz2), and sub-stage II (Qtz3), sphalerite from sub-stage I (Sp1) and sub-stage II (Sp2) and fluorite from sub-stage II (Fl) (Table 2). Both primary and secondary fluid inclusions are recognized in the Chomalu deposit. Secondary fluid inclusions occur along fracture planes and represent fluids trapped after host-mineral precipitation. Based on Roedder (1994), microthermometric measurements were carried out on the same fluid inclusion assemblages occurring in a primary single phase and evident growth zones. Only liquid-rich (L + V) type of fluid inclusions was identified based on their phases at room temperature (21 °C) (Roedder, 1984). They occur in the early stage and in the main stage (I and II) of mineralization, mainly as isolated individuals or locally in clusters. There was no evidence of daughter minerals, CO_2 and CH_4 in the fluid inclusions.

6.1. Early stage

Primary fluid inclusions in quartz samples (Qtz1) from the early stage, contain 20–30 vol% vapor, 6 to 20 μm size with elliptical, and rounded and irregular shapes (Fig. 10a). A total of fourteen primary fluid inclusions were studied in Qtz1, yield ice-melting temperatures (Tm-ice) of −2.9° to −2.0 °C, with corresponding salinities of 3.5 to 4.82 wt% NaCl equivalent based on Bodnar (1993) (Fig. 11). These FIAs have homogenization temperatures of 253° to 305 °C with an average of 275 °C (Fig. 11).

6.2. Main stage (sub-stage I)

Fluid inclusions in Qtz2 from base-metal ore are small (4–22 μm, mainly 8 to 12 μm; Fig. 10b), whereas in sphalerite from the base-metal ore (Sp1) are in range of 8 to 32 μm with a major clustering between 15 and 20 μm (Fig. 10c). They have elliptical, negative crystal, elongate and irregular shapes and contain 20 to 30 and 10 to 30 vol% vapor in Qtz2 and Sp1, respectively. Primary fluid inclusions in Qtz2 (total of 11 primary fluid inclusion) yield Tm-ice values in range of −2.8° to −1.2 °C, salinities of 2.18 to 4.65 wt% NaCl equivalent based on Bodnar (1993) (Fig. 11). These FIAs were completely homogenize to liquid phase at homogenization temperatures of 220° to 280 °C (average 250 °C) (Fig. 11). A total of 13 primary fluid inclusions were studied in Sp1, yield

Table 1
Electron microprobe results of the Chomalu epithermal deposit sulfide minerals, data in wt%. b.d: below detection limit. Abbreviations: Py, pyrite; Ccp, chalcopyrite; Gn, galena; Sp, sphalerite, Cv, covellite; Ttr, tetrahedrite.

		S	Fe	Cu	Zn	As	Ag	Cd	Au	Pb	Sb	Ga	Te	Bi	Ni	Sn	Total
Stage 1	Py	53.12	46.15	0.15	0.01	0.45	b.d	b.d	0.01	0.02	b.d	0.06	b.d	b.d	0.01	b.d	99.98
		53.24	46.57	0.12	0.05	0.15	b.d	b.d	b.d	0.13	b.d	b.d	b.d	b.d	0.14	b.d	100.40
		52.95	46.28	0.28	0.41	b.d	b.d	b.d	0.01	0.26	b.d	b.d	b.d	b.d	b.d	b.d	100.28
		52.21	46.31	0.21	b.d	0.02	b.d	b.d	b.d	b.d	b.d	b.d	b.d	b.d	0.38	b.d	99.13
	Ccp	34.19	31.18	33.85	0.02	0.01	b.d	b.d	b.d	0.45	b.d	b.d	b.d	b.d	0.16	b.d	99.86
		33.45	32.25	33.58	0.01	0.04	b.d	b.d	b.d	0.30	b.d	b.d	b.d	b.d	0.10	b.d	99.73
Sub-stage I	Gn	12.22	0.03	0.25	b.d	0.06	0.01	0.23	b.d	86.86	b.d	b.d	b.d	0.02	0.20	b.d	99.88
		10.24	0.17	8.99	b.d	0.02	0.06	0.04	b.d	80.39	b.d	b.d	b.d	0.15	0.08	b.d	100.14
		13.54	0.06	0.16	b.d	0.02	0.01	b.d	b.d	85.81	b.d	b.d	b.d	0.21	0.23	b.d	100.04
		12.64	0.14	0.20	b.d	0.04	0.01	0.55	b.d	86.66	b.d	b.d	b.d	0.01	b.d	b.d	100.25
		12.24	0.06	0.31	b.d	0.03	0.04	b.d	b.d	86.48	b.d	b.d	b.d	0.34	b.d	b.d	99.50
		12.47	0.06	0.84	b.d	0.07	0.09	b.d	b.d	85.32	b.d	0.15	b.d	0.28	0.48	b.d	99.76
		12.36	0.06	0.15	b.d	0.08	0.03	0.09	b.d	87.76	b.d	b.d	b.d	0.01	0.22	b.d	100.76
		10.00	0.09	3.04	b.d	0.04	0.02	0.05	b.d	86.78	b.d	b.d	b.d	0.09	0.12	b.d	100.23
	Sp	33.42	0.45	0.21	65.99	0.01	b.d	0.01	b.d	0.08	b.d	0.09	b.d	b.d	b.d	b.d	100.3
		33.49	0.28	b.d	66.72	b.d	0.04	0.01	b.d	b.d	b.d	b.d	b.d	b.d	b.d	b.d	100.5
		31.11	0.56	b.d	65.50	0.02	b.d	1.97	b.d	b.d	b.d	b.d	b.d	b.d	b.d	b.d	99.16
		32.74	0.34	b.d	65.80	b.d	0.02	0.02	b.d	0.04	b.d	0.14	b.d	b.d	b.d	b.d	99.10
		32.51	0.92	0.32	65.67	b.d	b.d	0.10	b.d	b.d	b.d	b.d	b.d	b.d	0.01	b.d	99.53
		32.73	0.17	b.d	67.35	b.d	0.05	0.01	b.d	b.d	b.d	b.d	b.d	b.d	b.d	b.d	100.3
		33.00	0.12	b.d	65.99	b.d	0.01	0.40	b.d	b.d	b.d	b.d	b.d	b.d	b.d	b.d	99.52
	Cv	30.50	0.08	63.23	0.28	b.d	5.43	b.d	b.d	b.d	b.d	b.d	b.d	b.d	b.d	b.d	99.52
		30.11	b.d	64.02	0.44	b.d	4.17	b.d	b.d	0.46	b.d	0.07	b.d	b.d	b.d	b.d	99.27
		30.10	0.30	63.97	0.53	b.d	3.97	b.d	b.d	0.66	b.d	0.04	b.d	b.d	b.d	b.d	99.57
		29.15	0.10	63.84	0.61	b.d	5.35	b.d	b.d	0.42	b.d	b.d	b.d	b.d	b.d	b.d	99.47
	Ccp	33.43	32.64	32.84	0.02	b.d	b.d	b.d	b.d	0.11	b.d	b.d	b.d	b.d	b.d	b.d	99.04
	Ttr	26.57	0.17	36.46	7.49	3.71	0.47	b.d	b.d	b.d	24.94	b.d	b.d	0.12	b.d	b.d	99.93
		25.25	0.14	36.95	7.24	4.02	1.49	b.d	b.d	b.d	25.03	0.08	b.d	b.d	b.d	b.d	100.20
		26.17	0.19	36.85	7.06	4.08	2.37	b.d	b.d	b.d	24.13	b.d	b.d	b.d	b.d	b.d	100.85
		25.60	0.15	37.16	6.85	4.16	0.56	b.d	b.d	b.d	24.59	b.d	b.d	b.d	b.d	b.d	99.07
Sub-stage II	Gn	12.73	0.10	b.d	b.d	b.d	b.d	b.d	b.d	86.85	b.d	b.d	0.01	0.33	b.d	b.d	100.02
		12.18	0.21	b.d	b.d	b.d	b.d	b.d	b.d	86.99	b.d	b.d	0.12	0.49	b.d	b.d	99.99
		13.19	0.06	0.10	b.d	b.d	b.d	b.d	b.d	86.16	b.d	b.d	0.06	0.61	0.31	b.d	100.49
		12.98	b.d	b.d	b.d	b.d	b.d	b.d	b.d	86.47	b.d	b.d	0.04	0.38	0.39	b.d	100.26
		13.47	0.08	b.d	b.d	b.d	b.d	b.d	b.d	86.00	b.d	b.d	0.07	0.41	0.20	b.d	100.23
		13.10	0.16	b.d	b.d	b.d	b.d	b.d	b.d	86.35	b.d	b.d	0.03	0.47	0.25	b.d	100.36
	Sp	33.35	0.83	b.d	65.16	b.d	b.d	b.d	b.d	0.16	0.02	b.d	b.d	0.30	b.d	b.d	99.82
		33.50	0.56	b.d	65.28	b.d	b.d	b.d	b.d	0.75	0.02	b.d	b.d	b.d	b.d	b.d	100.11
		32.31	0.62	b.d	66.74	b.d	b.d	b.d	b.d	0.06	0.07	b.d	b.d	0.14	b.d	b.d	99.94
		31.67	0.41	0.15	66.63	0.71	b.d	b.d	b.d	b.d	0.17	b.d	b.d	0.01	b.d	b.d	99.74

ice-melting temperatures (Tm-ice) of −3° to −1.8 °C, with corresponding salinities of 3.12 to 4.96 wt% NaCl equivalent based on Bodnar (1993), and homogenization temperatures of 200° to 237 °C with an average of 225 °C (Fig. 11).

6.3. Main stage (sub-stage II)

Fluid inclusion in Qtz3 FIAs from sub-stage II have elliptical, rounded and irregular shapes in range of 5–12 μm, with 10–25 vol% vapor (Fig. 10d). Salinities estimated for primary Qtz3 FIAs (a total of 7 fluid inclusion) are from 2.05 to 2.50 wt% NaCl equivalent (corresponding with Tm-ice of −1.4° to −1.1 °C) based on Bodnar (1993). Homogenization temperatures (Th) of Qtz3 FIAs are 180° to 230 °C (average 210 °C) (Fig. 11). Fluid inclusions in Fl from sub-stage II, have elliptical and rounded shapes of 9–36 μm in size, contain 10–25 vol% vapor (Fig. 10e). A total of 52 primary fluid inclusions were studied in Fl, yield ice-melting temperatures (Tm-ice) of −1.7° to −0.3 °C, with corresponding salinities of 0.53 to 2.90 wt% NaCl equivalent based on Bodnar (1993) (Fig. 11). These FIAs have homogenization temperatures of 187° to 229 °C with an average of 216 °C (Fig. 11). Primary FIAs from Sp2, composed of 10–40 vol% vapor phase of 10–107 μm size, mainly appear as elliptical, rounded, irregular and negative crystal shapes (Fig. 10f). Salinities estimated for primary Sp2 FIAs (a total of 15 fluid inclusion) are 1.74 to 2.57 wt% NaCl equivalent (corresponding with Tm-ice of −1.5° to −1 °C) with homogenization temperatures (Th) 183° to 235 °C (average 211 °C) (Fig. 11).

7. Discussion

7.1. Mineralization and fluid evolution

At Chomalu, fluid inclusions show that the early stage of mineralization formed over a range from 305° down to 253 °C with salinities between 4.8 down to 3.5 wt% NaCl equivalent. The subsequent main ore stage was characterized by generally lower homogenization temperatures of 200° to 280 °C and 180° to 235 °C with salinities of 2.18 to 4.96 and 0.53 to 2.90 wt% NaCl equivalent for sub-stages I and II, respectively. As noted before, there is no evidence for boiling, such as the coexistence of vapor and liquid dominated phase and also the absence of adularia and bladed calcite, as a main mechanism for gold and other ore precipitation (Simmons and Christenson, 1994; Simmons and Browne, 2000). Rapid cooling shown by the FIAs of each mineral generation, especially the main stage sphalerite, fluorite, and chalcedony in silicified veins, is the main trigger for ore precipitation. Precipitation of chalcedony can, however, be a product of rapid cooling possibly caused by boiling (Jiang et al., 2004).

The fluid evolution diagram, represented by homogenization temperature *vs.* salinity (Fig. 12; Wilkinson, 2001), suggests two main evolution stages with overlapping conditions. The main mechanism for ore precipitation at Chomalu was simultaneous dilution and cooling with oxidation state change (possibly accompanied by an increase in pH) by mixing a cold water (probably modified meteoric water) with hydrothermal fluid. Temperature decrease is one of the most commonly

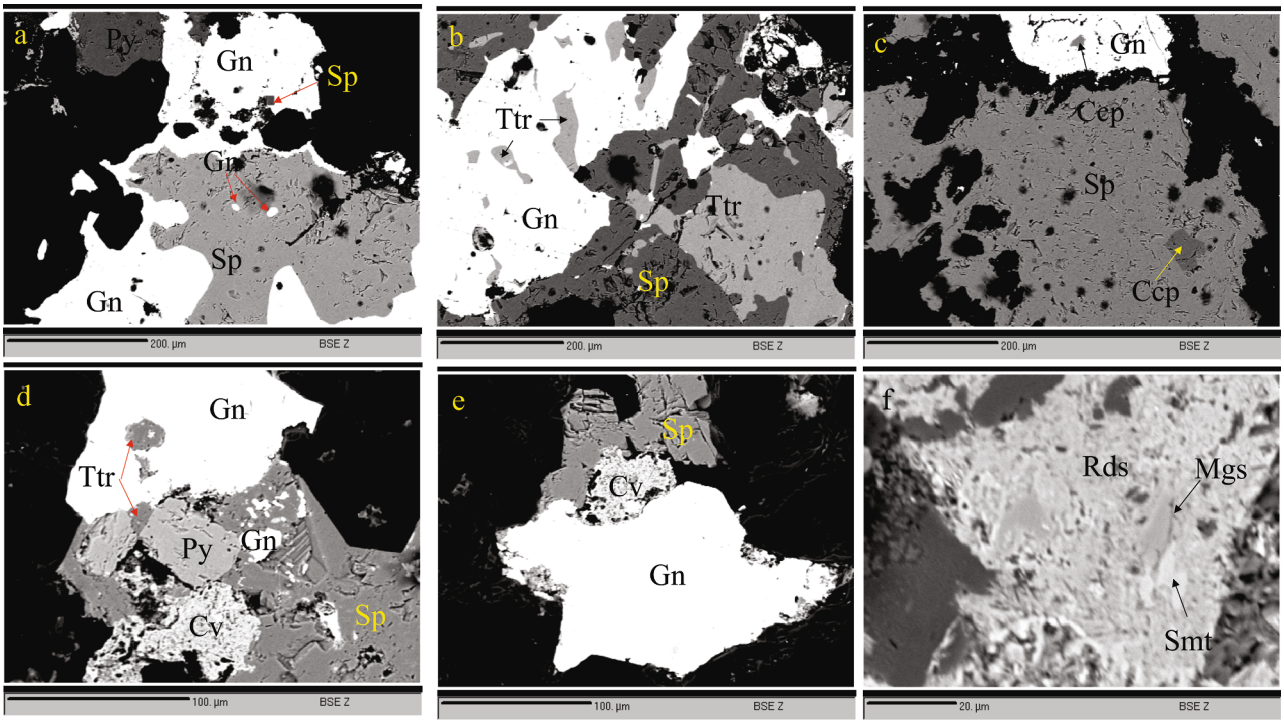

Fig. 9. SEM-BSE images of the Chomalu ore minerals: a) Inclusion of galena in sphalerite and sphalerite inclusion in galena of the sub-stage I; b and c) Inclusions of tetrahedrite and chalcopyrite in both galena and sphalerite of the sub-stage I; d and e) Ag-rich covellite formed by supergene oxidation in boundaries of galena and sphalerite of the sub-stage I, and a) Fe-Mn-Zn-Ca-Mg carbonates including mainly smithsonite, rhodochrosite and magnesite of the sub-stage III. Abbreviation: Py, pyrite; Ccp, chalcopyrite; Gn, galena; Sp, sphalerite, Cv, covellite; Ttr, tetrahedrite; Smt, smithsonite; Rds, rhodochrosite; Mgs magnesite.

Table 2
Summary of fluid inclusion data: Homogenization temperature (Th); ice melting temperature (Tm_{ice}); Salinity (wt.% NaCl), and Number of analyses (n).

Salinity (wt.% NaCl)	Th °(C)	Tm ice °(C)	Mineralization Stage	Host Mineral	Inclusion Type
3.5–4.82	253–305	−2 to −2.9	Early stage	Quartz (n = 14)	LV-type
2.18–4.65	220–280	−1.2 to −2.8	Main stage (sub-stage I)	Quartz (n = 11)	LV-type
3.12–4.96	200–237	−1.8 to −3	Main stage (sub-stage I)	Sphalerite (n = 13)	LV-type
2.05–2.50	180–230	−1.1 to −1.4	Main stage (sub-stage II)	Quartz (n = 7)	LV-type
1.74–2.57	183–235	−1 to −1.5	Main stage (sub-stage II)	Sphalerite (n = 15)	LV-type
0.53–2.90	187–229	−0.3 to −1.7	Main stage (sub-stage II)	Fluorite (n = 52)	LV-type

suspected processes leading to sulfide precipitation (Reed and Palandri, 2006; Fontboté et al., 2017). However, we conclude that simple temperature decrease is not the only mechanism initiating sulfide saturation with a temperature decrease resulting in dilution associated with cooling of hydrothermal fluid. In the early stage, Cu and possible Au (as electrum) precipitate close to intrusion at higher temperature of 305° decreasing to 253 °C and salinities of 4.8 decreasing to 3.5 wt% NaCl equivalent. The vast majority of metal precipitation (galena and sphalerite) results from greater dilution and cooling in the main stage (sub-stage I), which moves Ag from electrum to possibly argentite (see Reed and Palandri, 2006). Mineral assemblages (Zn-Mn-Fe-bearing carbonates) indicate changing redox from reduced in the early stage and sub-stages I and II to moderately oxidized conditions in the sub-stage III. In a Th *vs.* salinity diagram Roedder (1984), fluid inclusion data plot in the field of epithermal mineralization close to the magmatic fluid field with 0.78 to 0.93 g/cm^3 density (Fig. 12). The first ice melting in all of the inclusions begins at temperatures of −29.5° up to −21.2° C (average −23.5° C), implying the dominance of the NaCl–H_2O system during mineralization. Due to an insignificant role of boiling at Chomalu, for pressure corrections we assume an average thickness of the volcanic rocks of 800 m, which is equal to 200 bar. Correction at 200 bar, based on Bodnar (1993) and Steele-MacInnis et al. (2012), adds up to 10–12 °C to the corresponding measured Th as the best estimate of trapping temperatures. Therefore, the depth of formation of mineralization at Chomalu probably was 300 to 700 m below the paleosurface, consistent with IS deposits found within vertical intervals generally of 300–800 m (e.g., Hedenquist et al., 2000; Albinson and Nelson, 2001; Echavarria et al., 2006).

7.2. Genesis and ore deposition model

Porphyry Cu-Mo-Au deposits, polymetallic epithermal deposits, Cu, Cu-Fe, Au, and Zn-Pb skarn deposits, Cordilleran polymetallic veins and replacement bodies, and distal Au deposits form in magmatic-hydrothermal systems in association with magmatic arcs (Henley and Berger, 2013; Pirajno, 2015). Polymetallic epithermal deposits form at less than ~1.5 km depth and temperatures range of 150° to 300 °C (e.g., Hedenquist et al., 2000; Simmons et al., 2005), and are subdivided into HS, IS, and LS types. Features and characterization of these epithermal types are discussed comprehensively in the literature (e.g., White and Hedenquist, 1990; Einaudi et al., 2003; Wang et al., 2019). In this section, we compare the most significant features of the deposit, such as ore and gangue mineralogy, ore texture, tectonic settings, relation to magmatism and the sulfidation state of epithermal deposits, then we present a schematic and simplified scenario for ore deposition in the Chomalu deposit.

Enargite-luzonite-famatinite-covellite mineral assemblages, high content of sulfides (10–90 vol%), quartz-alunite, quartz-pyrophyllite,

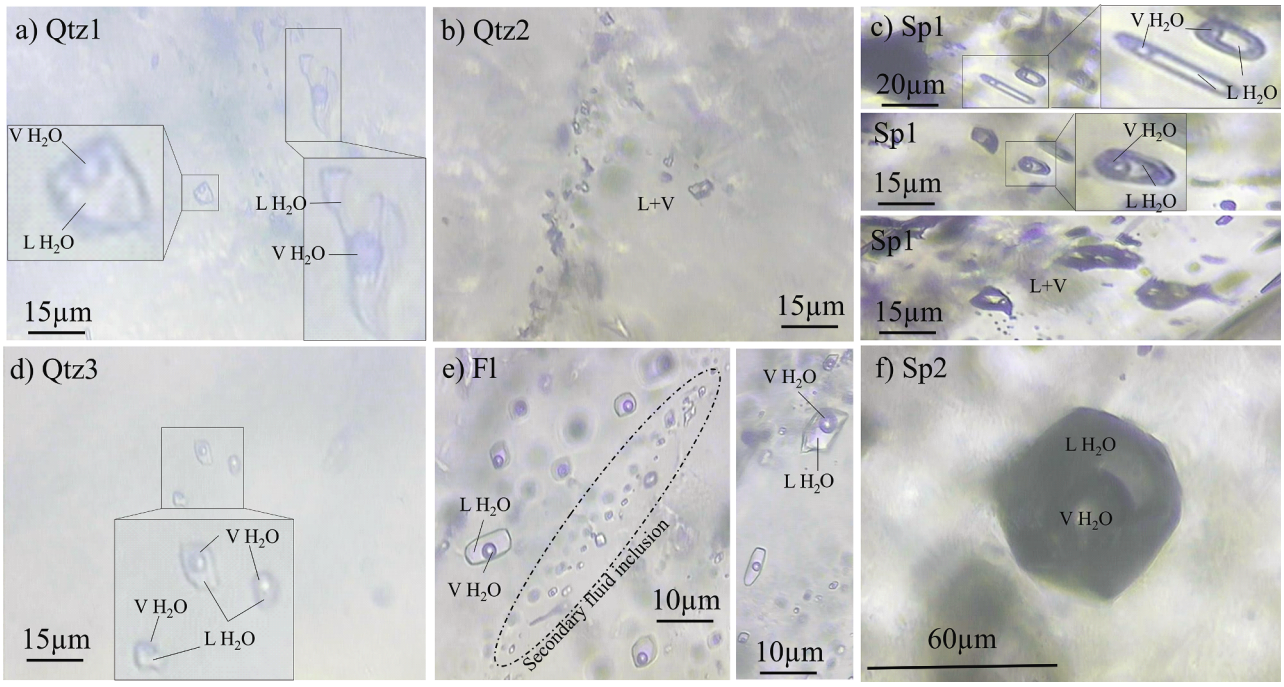

Fig. 10. Photomicrographs of fluid inclusions in the Chomalu ore veins: a) Liquid-rich fluid inclusions in early stage quartz (Qtz1); b) Fluid inclusions in sub-stage I quartz (Qtz2); c) Primary fluid inclusions in sub-stage I sphalerite (Sp1) with elliptical, rounded and irregular shapes; d) Primary fluid inclusions in sub-stage II quartz (Qtz3); e) Primary and secondary fluid inclusions in sub-stage II fluorite (Fl), f) Primary fluid inclusions in sub-stage II sphalerite (Sp2).

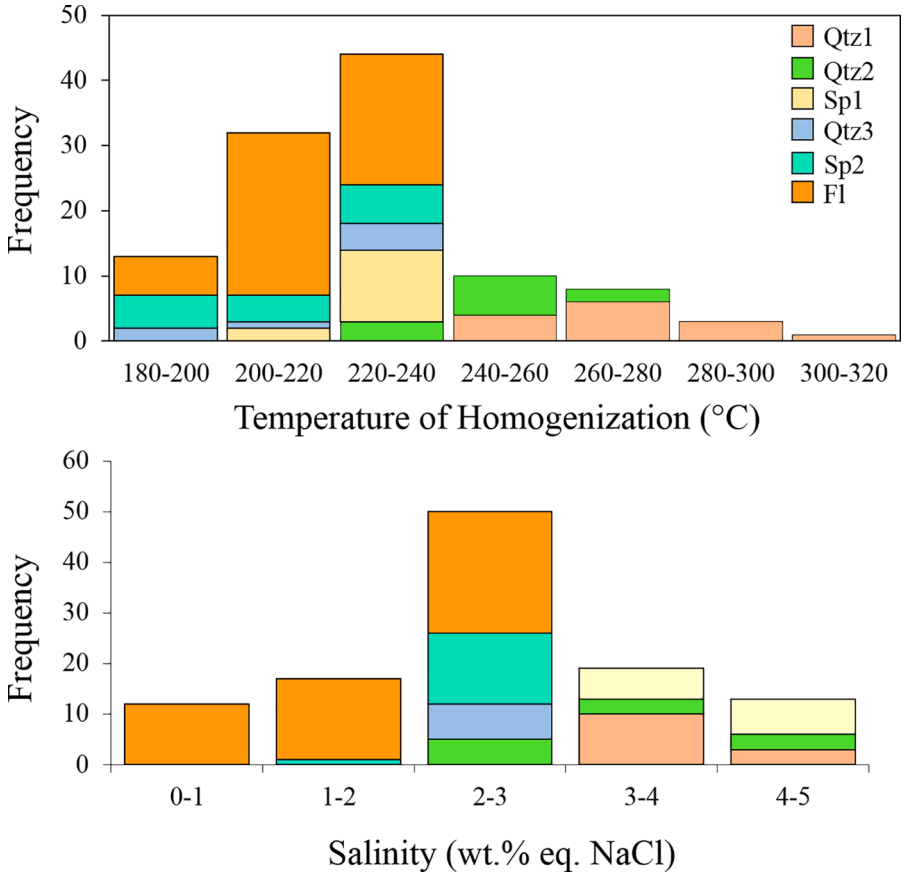

Fig. 11. Histograms of homogenization temperatures and salinities for primary fluid inclusions in the Chomalu ore veins. Mineral abbreviations and paragenetic stage are as follows: sphalerite (Sp1 and Sp2 from sub-stages I and II, respectively), quartz (Qtz1, Qtz2 and Qtz3 from early stage and sub-stages I and II, respectively), fluorite (Fl from sub-stage II).

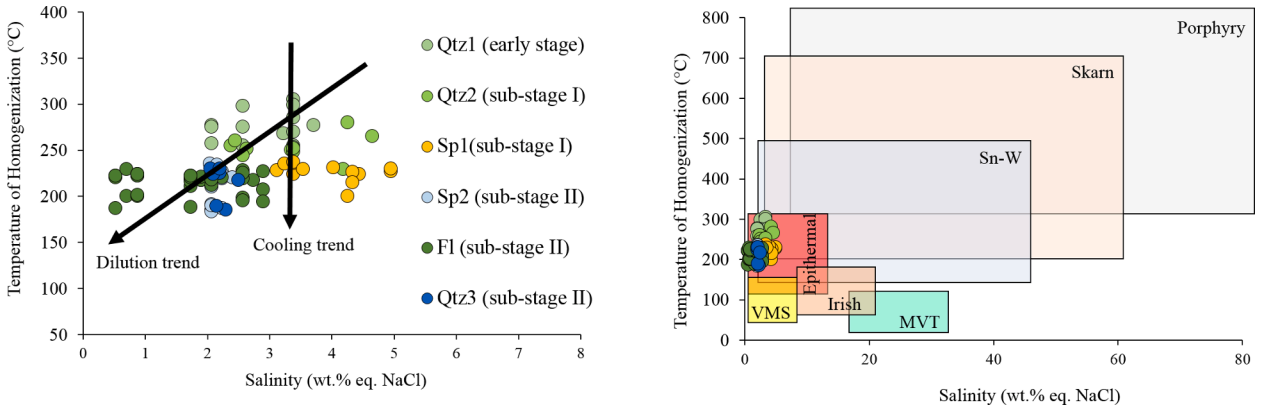

Fig. 12. Th *vs.* salinity plot of fluid inclusion data showing fluid dilution trend and deposit type based on Wilkinson (2001).

and quartz-dickite alteration mineral assemblages and barite as the main gangue mineral in the absence of carbonate, are key features of the HS type, whereas abundant arsenopyrite, low sulfides content (typically <2 vol%), minor pyrite, chalcedony-quartz ± carbonate ± fluorite as primary gangue minerals, and illite/smectite-adularia as alteration minerals are key features of the LS type. Mineral assemblages in the Chomalu ore veins is relatively simple, including pyrite, arsenopyrite, Fe-poor sphalerite, galena, chalcopyrite, bornite, tetrahedrite, and Zn-Mn-Fe carbonate mineral are similar to the majority of IS deposits (Einaudi et al., 2003; Sillitoe and Hedenquist, 2003; Wang et al., 2019). The gangue minerals in IS deposits are typically quartz, Mn-carbonates, commonly rhodochrosite and manganoan calcite, and fluorite (Wang et al., 2019 and references therein). Quartz, fluorite, rhodochrosite, and calcite are the main gangue minerals in the Chomalu deposit. Hydrothermal alteration at Chomalu included intensive silicification in the first mineralized zone associated with minor sericitization and intensive argillization (kaolinite and illite) and propylitization in the second mineralized zone.

Key features in the Chomalu deposit are: 1) pyrite, sphalerite, galena, tetrahedrite, chalcopyrite, minor arsenopyrite and abundant Zn-Mn-Fe carbonate minerals; 2) high content of silver and base metals with high silver to gold ratios (50–60); 3) a sulfide content of ~40 vol% in the veins; 4) proximal sericite alteration and distal kaolinite and illite alteration (adularia absence), and 5) presence of crustiform banding, vuggy and veins and brecciated bodies. These features suggest that the Choumalu is an IS epithermal deposit (Sillitoe and Hedenquist, 2003; Wang et al., 2019).

The weak zonation, characterized by the formation of Cu-Au-Fe mineral assemblages in the first mineralized zone, followed by an increase in Pb-Zn ± Ag toward west and north, and finally precipitation of Zn-Fe-Mn carbonate in the northern part of the district, indicates that the early fluid that formed Cu-Au-Fe assemblages possibly originated from the intrusion and then migrated outward into the volcanic complex. In the first mineralized zone fluids formed E-W trending veins along a major fault in the host andesites. As they flowed upward and encountered several subordinate faults (mainly NW-SE faults), the second mineralized zone formed, roughly parallel to the faults. Fluid of the main ore-stage overprinted the early-stage ore and continued to flow to the north and west. Einaudi et al. (2003) present a diagram for the sulfidation state of sulfides as a function of high fS_2 and intermediate to low fO_2 and temperature (1000/T) showing that IS type sulfidation is stable with respect to chalcopyrite-pyrite-argentite, as well as tennantite and tetrahedrite. The Chomalu ore assemblages trace slight fluctuations in terms of sulfidation state (Fig. 13). The FeS content in sphalerite increases slightly from 0.12 to 0.92 wt% (average 0.40 wt%) in sub-stage I to 0.41–0.83 wt% (average 0.60 wt%) in sub-stage II, implying a slight decrease in sulfidation state accompanied by an increase in pH. The latter is indicated by sericite and vuggy quartz deposition in the early

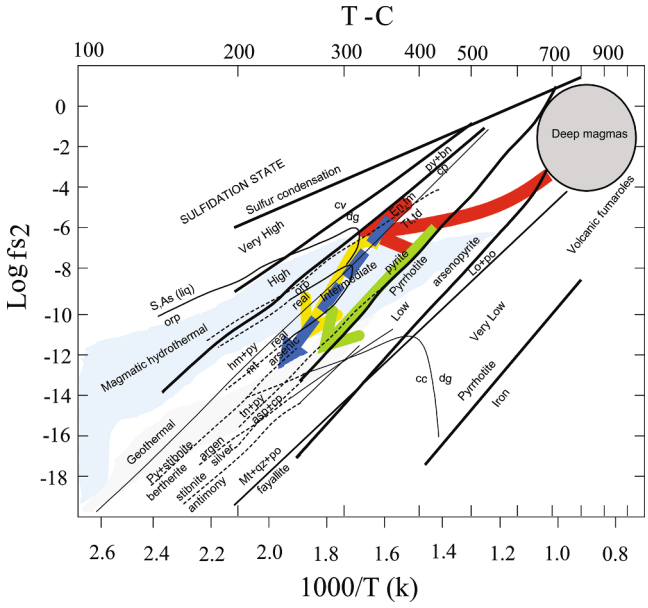

Fig. 13. Sulfidation state in the epithermal-porphyry systems according to LogfS_2 *vs* T (°C) diagram (Einaudi et al., 2003). Red arrow indicates porphyry copper deposits; yellow arrow indicates intermediate-sulfidation precious-base metal veins associated with porphyries, and green arrow reflects sulfidation evolution for the La Guitarra and other similar epithermal deposits (Camprubí and Albinson, 2007). Blue dashed line represents fluid evaluation and decrease in the sulfidation evolution from Glojeh to Chomalu deposits.

stage and increasing argillic alteration with kaolinite and illite in sub-stage I and II, and finally siderite and other carbonate minerals in the sub-stage III. Widespread precipitation of Zn-Fe-Mn carbonate in the outer sphalerite-galena zone may indicates an increase in oxidation state.

In terms of tectonic settings and age of mineralization, these IS deposits can develop in all stress regimes (compressive, neutral, and extensional) in magmatic arcs (Sillitoe and Hedenquist, 2003), back arcs (Camprubí and Albinson, 2007), and post-collisional orogenic belt (Xie et al., 2017). They are mainly of Cenozoic age with a distinct peak in the Miocene (Wang et al., 2019). IS type deposits are commonly hosted by andesitic volcanic rocks, which may be comagmatic with the causative porphyry intrusion. The Chomalu deposit formed in the Eocene extensional setting within andesite to olivine basalt host, and fluid inclusions microthermometry indicates that hydrothermal fluids made a contribution to the ore mineralization. In addition, intermediate sulfidation epithermal deposits are divided into two sub-classes, namely Neutral-Compressional IS (NC-type IS) and Extensional IS (E-type IS) (refer to

Wang et al., 2019 for more details). Western Alborz Magmatic Arc and Alborz-Azerbaijan Magmatic Belt are considered as an extensional back-arc tectonic setting (Fig. 14a; Shafaii Moghadam et al., 2020; Ghasemi Siani et al., 2020). The Chomalu deposit formed in an extensional setting with Ag-Pb-Zn and high Ag/Au metal (50–60) associations and is therefore considered as an E-type IS deposit. A generalized model for mineralization in the Chomalu deposit shows that at 39 to 40 Ma (unpublished U-Pb age and Ar-Ar ages by Ghasemi Siani et al., 2015); the intrusive center acted as the heat engine and source of hydrothermal fluid in close vicinity of the mineralized zones. Unfortunately, we cannot directly verify the timing of mineralization due to the absence of good representative sericite. After intrusion, exsolving magmatic hydrothermal fluids extracted Cl, S, Au, and Ag from sulfides and the silicate melt, developing a saline ore-bearing fluid system (H_2O-NaCl), enriched in metals and sulfur as chloride and bisulfide complexes (refer to Zhu et al., 2011). The released metal-bearing hydrothermal fluid migrated upwards and laterally to the north and west, and after extracting more metals, such as Pb and Zn from volcanic rocks, mixed with meteoric water, causing a rapid decrease in temperature and resulting in ore precipitation as open space (faults) filling (Fig. 14b).

7.3. Comparison with Cordilleran ore types and future exploration guide

Polymetallic epithermal ore deposits were initially classified as Cordilleran vein-type deposits formed in veins or lodes in porphyry-related systems (Bendezú and Fontboté, 2002; Bendez et al., 2003; Bendezu and Fontbote, 2009; Fontboté et al., 2009). Einaudi (1982), Bendezú et al. (2008), and Baumgartner et al. (2008) use the term polymetallic\base -metal epithermal deposits. This type of mineralization has also been termed "zoned base-metal veins" by Einaudi et al. (2003), but a clear zonation is not always recognizable. Some key features of Cordilleran base-metal deposits include (modified after Bendezu et al., 2008; Bendezu and Fontbote, 2009): 1) close association in time and space with calc-alkaline igneous activity, i.e. same environment as most porphyry Cu and HS epithermal Au–Ag deposits; 2) precipitation mostly under epithermal conditions at temperatures <375 °C and moderate to low salinity (e.g., Kouzmanov et al., 2004; Prendergast et al., 2005; Bendezú, 2007; Baumgartner et al., 2008; Catchpole et al., 2009; Rusk et al., 2008; Catchpole et al., 2011); 3) sulfides rich base-metal veins (up to more than 50 wt% total sulfides); 4) mostly well-developed zoning of ore and alteration minerals with HS (advanced argillic alteration assemblages) in the core followed by an early pyrite–quartz stages that can be extensive and form large zoned bodies outwardly as Zn–Pb ores; 5) mainly as open-space fillings (veins, breccia bodies) in silicate host rocks and as replacement in carbonate rocks; and 6) higher Ag/Au ratios than HS epithermal Au–(Ag) mineralization. Cordilleran ore deposits are also subdivided into strongly zoned and weakly zoned deposits. Strongly zoned deposits like Smelter-Colquijirca (Baumgartner et al., 2008; Bendezu and Fontbote, 2009) are characterized by enargite, pyrite, quartz ± (tennantite, wolframite, chalcopyrite, covellite, chalcocite, alunite, dickite, kaolinite) in the internal sector and sphalerite, galena ± (sericite, kaolinite, dickite, hematite, Mn-Fe carbonates) in the external part, whereas in the weakly zoned deposits (such as Domo de Yauli, Beuchat et al., 2004; Cerro de Pasco, Baumgartner et al., 2008; Morococha, Catchpole, 2011; Catchpole et al., 2012; Catchpole et al., 2015), pyrrhotite, pyrite, quartz ± (chalcopyrite, arsenopyrite, tetrahedrite, carbonates, sericite, chlorite) form in internal part, whereas external zones are characterized by sphalerite, galena, and pyrrhotite ± (Mn-Fe carbonates, sericite, chlorite, quartz).

Many of the Cordilleran ore deposits features are present in the Chomalu epithermal system, for example 1) the Chomalu deposit formed close the Varmarziar high-K, I-type intrusion; 2) presence of Cu porphyry in Rashtabad and Chodarchay indicates (Yasami et al., 2017) a possible association of porphyry-epithermal ore systems in the THMP; 3) low to moderate homogenization temperatures of 187° to 305 °C and low to moderate salinities of 0.53 to 4.96 wt% NaCl equivalent; and 4) high sulfide content (40 %) and high Ag/Au (50–60). As noted above, the geometry, mineralogical patterns, and paragenetic sequence of the orebodies at Chomalu are consistent with the weakly zoned Cordilleran system. The early stage, with sericite reflecting acidic conditions and the assemblage of pyrite, quartz, chalcopyrite, arsenopyrite, and bornite, is comparable to the internal sector of weakly zoned base-metal deposits, whereas external parts of the main stage, characterized by kaolinite and illite associated with sphalerite, galena and Zn-Mn-Fe carbonates, are consistent with external part of the weakly zoned Cordilleran system. On the regional scale, the Glojeh deposit, located in the west of the Chomalu deposit, has an internal part with enargite, famatinite, chalcocite, covellite, bournonite, chalcopyrite, bornite, and pyrite assemblages implying HS state, and margins with Ag-rich sphalerite-galena bodies suggesting an IS state, these features are consistent with strongly zoned base-metal deposits (Cordilleran type ore vein).

Presence of both strongly and weakly zoned Cordilleran-type ore veins indicate that mineralizing fluids were strongly fluctuating in pH and sulfidation states from high sulfidation states in the central part of north Glojeh vein to intermediate sulfidation state in the periphery area (south Glojeh and Chomalu), which depend on temperature and spatial path followed by the ore-forming fluids and their interaction with the host rocks (e.g., Baumgartner et al., 2008). Although our previous research indicates that extensional back-arc magmatic activity of the THMP is less prospective for porphyry deposits, although there is evidence of porphyry mineralization in the Chodarchay (Yasami et al., 2017) and Glojeh deposits (Mehrabi et al., 2016), as well as similarities between these deposits with Cordilleran-type ore veins suggesting that it is possible to find porphyry deposits in the THMP.

8. Concluding remarks

The Chomalu polymetallic epithermal deposit is located in the THMP, close to the Varmarziar high-K, I-type granitic batholith. Ore

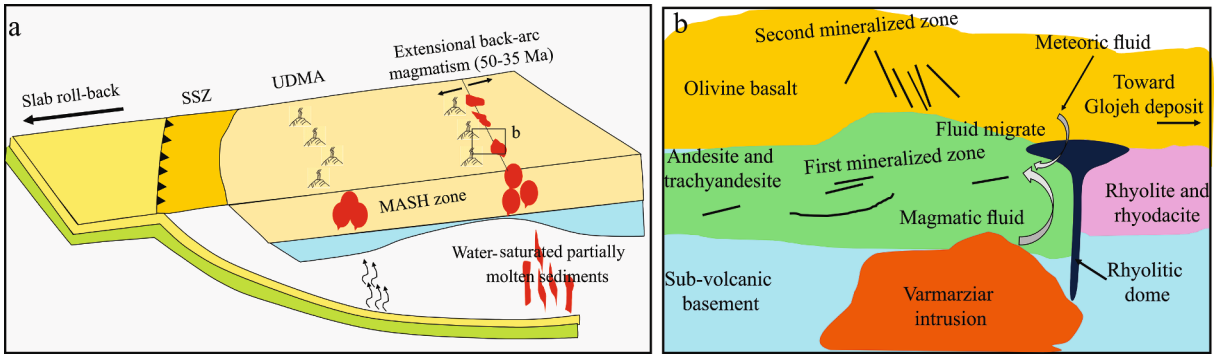

Fig. 14. Simplified geological model of the THMP tectonic settings (a), and Chomalu ore mineralized veins (b).

mineralization in the Chomalu veins consist of early Au-Cu, followed by Ag-Pb-Zn and finally Zn-Mn-Fe carbonate assemblages. A supergene stage can be found near surface. Metal sulfide precipitation is driven largely by the temperature decrease and concomitant destabilizing chloride-metal complexes, which was caused by dilution and cooling of ore-bearing fluids. The Chomalu polymetallic epithermal deposit is classified as an IS epithermal deposit formed in an extensional back-arc tectonic setting associated with high-K alkalic I-type plutonism, which is comparable with weakly zoned Cordilleran-type epithermal polymetallic mineralization. Due to occurrences of both weakly and strongly zoned Cordilleran-type epithermal in the same area, and development of numerous epithermal ore deposits, THMP can be considered as major target area for further exploration of silver-rich epithermal deposits and possibly porphyry Cu-Mo deposits.

Declaration of Competing Interest

The authors declare that they have no known competing financial interests or personal relationships that could have appeared to influence the work reported in this paper.

Acknowledgments

We acknowledge financial support of the Geological Survey of Iran (GSI), Iranian Mineral Processing Research Center (IMPRC) and Kharazmi University of Tehran, Iran. Authors are very grateful to Prof. David Lentz (University of New Brunswick) for a thorough review of earlier versions of the manuscript and English editing. Editor Prof. Huayong Chen is thanked for his advice and devoted editorial handling. Reviews by two anonymous reviewers helped clarifying our descriptions and interpretations and improved the paper tremendously.

References

Aghajani, S., Emami, M.H., Lotfi, M., Gholizadeh, K., Ghasemi Siani, M., 2016. Source of polymetal epithermal veins at Nikuyeh district (West of Qazvin) based on mineralogy, alteration and fluid inclusion studies. Scientific Quarterly Journal, Geosciences 25, 157–168. In Persian with English abstract.

Albinson, T., Nelson, C.E. (Eds.), 2001. New Mines and Discoveries in Mexico and Central America. Society of Economic Geologists, pp. 1–32. https://doi.org/10.5382/SP.08.01.

Azizi, H., Jahangiri, A., 2008. Cretaceous subduction-related volcanism in the northern Sanandaj-Sirjan Zone. Iran. J. Geodyn. 45 (4-5), 178–190.

Baumgartner, R., Fontbote, L., Vennemann, T., 2008. Mineral zoning and geochemistry of epithermal polymetallic Zn-Pb-Ag-Cu-Bi mineralization at Cerro de Pasco. Peru. Econ. Geol. 103 (3), 493–537.

Bendezú, R., 2007. Shallow polymetallic and precious metal mineralization associated to a Miocene diatreme-dome complex of the Peruvian Andes: The Colquijirca district. Université de Genève. PhD Theses. doi: 10.13097/archive-ouverte/unige.

Bendezú, R., Fontboté, L., 2002. Late timing for high-sulfidation Cordilleran base metal lode and replacement deposits in porphyry-related districts: the case of Colquijirca, central Peru. Society for Geology Applied to Mineral (SGA). News 13, 9–13.

Bendezu, R., Fontbote, L., 2009. Cordilleran epithermal Cu-Zn-Pb-(Au-Ag) mineralization in the Colquijirca district, Central Peru: Deposit-scale mineralogical patterns. Econ. Geol. 104 (7), 905–944.

Bendez, R., Fontbot, L., Cosca, M., 2003. Relative age of Cordilleran base metal lode and replacement deposits, and high-sulfidation Au-(Ag) epithermal mineralization in the Colquijirca mining district, central Peru. Miner. Deposita. 38 (6), 683–694.

Beuchat, S., Moritz, R., Pettke, T., 2004. Fluid evolution in the W-Cu-Zn-Pb San Cristobal vein, Peru: Fluid inclusion and stable isotope evidence: Chem. Geol. 210 (1-4), 201–224.

Bodnar, R.J., 1993. Revised equation and table for determining the freezing point depression of H_2O-NaCl solutions. Geochim. Cosmochim. Act. 57 (3), 683–684.

Camprubí, A., Albinson, T., 2007. Epithermal deposits in Mexico–update of current knowledge, and an empirical reclassification. Spec. Pap. Geol. Soc. Am. 422, 377–415.

Catchpole, H., 2011. Porphyry-related polymetallic mineralization in the Morococha district, central Peru: mineralization styles, timing and fluid evolution. PhD Theses. Université de Genève. doi: 10.13097/archive-ouverte/unige.

Catchpole, H., Kouzmanov, K., Fontbote, L., 2012. Copper-excess stannoidite and tennantite-tetrahedrite as proxies for hydrothermal fluid evolution in a zoned cordilleran base metal district, Morococha, Central Peru. Can. Mineral. 50 (3), 719–743.

Catchpole, H., Kouzmanov, K., Fontboté, L., Guillong, M., Heinrich, C.A., 2011. Fluid evolution in zoned Cordilleran polymetallic veins – Insights from microthermometry and LA-ICP-MS of fluid inclusions. Chem. Geol. 281 (3-4), 293–304.

Catchpole, H., Kouzmanov, K., Fontboté, L., Guillong, M., Heinrich, C.A., 2009. Fluid evolution in base metal veins a FI microthermometry and LA-ICP-MS case study: ECOFRI. Granada.

Catchpole, H., Kouzmanov, K., Putlitz, B., Seo, J.H., Fontbote, L., 2015. Zoned base metal mineralization in a porphyry system: origin and evolution of mineralizing fluids in the Morococha district. Peru. Econ. Geol. 110 (1), 39–71.

Echavarria, L., Nelson, E., Humphrey, J., Chavez, J., Escobedo, L., Iriondo, A., 2006. Geologic evolution of the Caylloma epithermal vein district, southern Peru. Econ. Geol. 101 (4), 843–863.

Einaudi, M.T., Hedenquist, J.W., Inan, E.E., 2003. Sulfidation state of fluids in active and extinct hydrothermal systems: transitions from porphyry to epithermal environments. In: Simmons, S.F., Graham, I. (Eds.), Volcanic, Geothermal, and Ore-Forming Fluids: Rulers and Witnesses of Processes within the Earth. Soc. Econ. Geol. Spec. Publ. 10, 285–313.

Esmaeli, M., Lotfi, M., Nezafati, N., 2015. Fluid inclusion and stable isotope study of the Khalyfehlou copper deposit, southeast Zanjan. Iran. Arab. J. Geosci. 8 (11), 9625–9633.

Faridi, M., Anvari, A., 2005. Geological Map of Hashtjin at the scale 1:100,000. Geological Survey of Iran.

Fontboté, L., Bendezú, R., 2009. Cordilleran or Butte-type Veins and Replacement Bodies as a Deposit Class in Porphyry Systems. In: Williams, P.J. (Ed.), Proceedings of the 10th Biennial Society of Geology Applied to Ore Deposits Meeting.

Fontboté, L., Kouzmanov, K., Chiaradia, M., Pokrovski, G.S., 2017. Sulfide minerals in hydrothermal deposits. Elements 13 (2), 97–103.

Ghasemi Siani, M., Lentz, D.R., Nazarian, M., 2020. Geochemistry of igneous rocks associated with mineral deposits in the Tarom-Hashtjin metallogenic province, NW Iran: An analysis of the controls on epithermal and related porphyry-style mineralization. Ore Geol. Rev. 126, 103753. https://doi.org/10.1016/j.oregeorev.2020.103753.

Ghasemi Siani, M., Lentz, D.R., 2022. Lithogeochemistry of various hydrothermal alteration types associated with precious and base metal epithermal deposits in the Tarom-Hashtjin metallogenic province, NW Iran: Implications for regional exploration. J. Geochem. Explor. 232, 106903. https://doi.org/10.1016/j.gexplo.2021.106903.

Ghasemi Siani, M., Mehrabi, B., Azizi, H., Wilkinson, C.M., Ganerod, M., 2015. Geochemistry and geochronology of the volcano-plutonic rocks associated with the Glojeh epithermal gold mineralization, NW Iran. Open Geosciences 7, 207–222.

Hedenquist, J.W., Arribas, A., Reynolds, T.J., 1998. Evolution of an intrusion-centered hydrothermal system: Far Southeast-Lepanto porphyry and epithermal Cu-Au deposits. Philippines. Econ. Geol. 93 (4), 373–404.

Hedenquist, J.W., Arribas, A., Urien-Gonzalez, E., 2000. Exploration for epithermal gold deposits. In: Hagemann, S.G., Brown, P.E. (Eds.), Gold in 2000. Soc. Econ. Geol. Rev. Econ, Geol, pp. 245–277.

Hemley, J.J., Hunt, J.P., 1992. Hydrothermal ore-forming processes in the light of studies in rock-buffered systems: II. Some general geologic applications. Econ. Geol. 87 (1), 23–43.

Henley, R.W., Adams, D.P.M., 1992. Strike-slip fault reactivation as a control on epithermal vein-style gold mineralization. Geology 20 (5), 443. https://doi.org/10.1130/0091-7613(1992)020<0443:SSFRAA>2.3.CO;2.

Henley, R.W., Berger, B.R., 2013. Nature's refineries–Metals and metalloids in arc volcanoes. Earth-Sci. Rev. 125, 146–170.

Jiang, S.H., Nie, F.J., Zhang, Y., Hu, P., 2004. The latest advances in the research of epithermal deposits. Earth Science Frontiers 11, 401–411.

Kouhestani, H., Azimzadeh, A.M., Mokhtari, M.A.A., Ebrahimi, M., 2017. Mineralization and fluid evolution of epithermal base metal veins from the Aqkand deposit. NW Iran. J. Mineral. Geochem. 194 (2), 139–155.

Kouhestani, H., Mokhtari, M.A.A., Chang, Z., Johnson, C.A., 2018. Intermediate sulfidation type base metal mineralization at Aliabad-Khanchy, Tarom-Hashtjin metallogenic belt. NW Iran. Ore Geol. Rev. 93, 1–18.

Kouzmanov, K., Ramboz, C., Bailly, L., Bogdanov, K., 2004. Genesis of high-sulphidation vinciennite-bearing Cu-As-Sn (±Au) assemblage from the Radka epithermal copper deposit, Bulgaria: evidence from mineralogy and infrared microthermometry of enargite. Can. Mineral. 42, 1501–1521.

Mehrabi, B., Siani, M.G., 2012. Intermediate sulfidation epithermal Pb-Zn-Cu (±Ag-Au) mineralization at Cheshmeh Hafez deposit, Semnan Province. Iran. J. Geol. Soc. Ind. 80 (4), 563–578.

Mehrabi, B., Tale Fazel, E., Ghasemi Siani, M., Eghbali, M.A., 2010. Investigation on mineralization and genetic model of Gulojeh Cu-Au vein deposit (north of Zanjan), using mineralogical, geochemical and fluid inclusion data. Journal of Sciences 35 (4), 185–199. In Persian with English abstract.

Mehrabi, B., Siani, M.G., Goldfarb, R., Azizi, H., Ganerod, M., Marsh, E.E., 2016. Mineral assemblages, fluid evolution, and genesis of polymetallic epithermal veins, Glojeh district. NW Iran. Ore Geol. Rev. 78, 41–57.

Mikaeili, K., Hosseinzadeh, M.R., Moayyed, M., Maghfouri, S., 2018. The Shah-Ali-Beiglou Zn-Pb-Cu(-Ag) Deposit, Iran: An example of intermediate sulfidation epithermal type mineralization. Minerals 8, 148. https://doi.org/10.3390/min8040148.

Mousavi Motlagh, S.H., Ghaderi, M., 2019. The Chargar Au-Cu deposit: an example of low sulfidation epithermal mineralization from the Tarom subzone, NW Iran. J. Mineral. Geochem. 196, 43–66.

Muntean, J.L., Einaudi, M.T., 2001. Porphyry-epithermal transition: Maricunga Belt, northern Chile. Econ. Geol. 96, 743–772.

Prendergast, K., Clarke, G.W., Pearson, N.J., Harris, K., 2005. Genesis of pyrite-Au-As-Zn-Bi-Te zones associated with Cu-Au skarns: evidence from the Big Gossan and Wanagon gold deposits, Ertsberg District, Papua. Indonesia. Econ. Geol. 100, 1021–1050.

Reed, M.H., Palandri, J., 2006. Sulfide mineral precipitation from hydrothermal fluids. Rev. Mineral. Geochem. 61, 609–631.
Richards, J.P., 2015. Tectonic, magmatic, and metallogenic evolution of the Tethyan orogen: From subduction to collision. Ore. Geol. Rev. 70, 323–345.
Richards, J.P., Spell, T., Rameh, E., Razique, A., Flectcher, T., 2012. High Sr/Y magmas reflect arc maturity, high magmatic water content, and porphyry Cu ± Mo ± Au potential: Examples from the Tethyan arcs of central and eastern Iran and western Pakistan. Econ. Geol. 10, 295–332.
Roedder, E., 1984. Fluid inclusions. Reviews in Mineralogy 12. Mineralogical Society of America, Washington, p. 644 p..
Rusk, B.G., Miller, B.J., Reed, M.H., 2008. Fluid inclusion evidence for the formation of Main Stage polymetallic base-metal veins, Butte, Montana, USA. (J.E. Spencer and S. R. Titley, eds.). Arizona Geological Survey, Tucson, Arizona Geological Society Digest 22, 573–581.
Schettino, A., Turco, E., 2011. Tectonic history of the western Tethys since the Late Triassic. Geol. Soc. Am. Bull. 123, 89–105.
Shafaii Moghadam, H., Li, Q.L., Li, X.H., Stern, R.J., Levresse, G., Santos, J.F., Lopez Martinez, M., Ducea, M.N., Ghorbani, G., Hassannezhad, A., 2020. Neotethyan subduction ignited the Iran arc and back-arc differently. Journal of Geophysical Research: Solid Earth, doi:10.1029/2019JB018460.
Shamanian, G.H., Hedenquist, J.W., Hattori, K.H., Hassanzadeh, J., 2004. The Gandy and Abolhassani epithermal prospects in the Alborz magmatic arc, Semnan Province, northern Iran. Econ. Geol. 99, 691–712.
Sillitoe, R.H., 2010. Porphyry copper systems. Econ. Geol. 105, 3–41.
Sillitoe, R.H., Hedenquist, J.W., 2003. Linkages between volcanotectonic settings, ore fluid compositions, and epithermal precious metal deposits. In: Simmons, S.F., Graham, I. (Eds.), Volcanic, Geothermal, and Ore-Forming Fluids: Rulers and Witnesses of Processes within the Earth. Publ, Soc. Econ. Geol. Spec, pp. 315–343.
Simmons, S.F., Browne, P.R.L., 2000. Hydrothermal minerals and precious metals in the Broadlands-Ohaaki geothermal system: implications for understanding low sulfidation epithermal environments. Econ. Geol. 95, 971–999.
Simmons, S.F., Christenson, B.W., 1994. Origins of calcite in a boiling geothermal system. Am. J. Sci. 294, 361–400.
Simmons, S.F., White, N.C., John, D.A., 2005. Geological characteristics of epithermal precious and base metal deposits. Econ. Geol. 485–522 100th Anniversary Volume.
Steele-MacInnis, M., Lecumberri-Sanchez, P., Bodnar, R.J., 2012. HOKIEFLINCS, H_2O-NaCl: A Microsoft Excel spreadsheet for interpreting microthermometric data from fluid inclusions based on the PVTX properties of H_2O-NaCl. Computers and Geosciences 49, 334–337.
Tale Fazel, E., Mehrabi, M., Ghasemi Siani, M., 2019. Epithermal systems of the Torud-Chah Shirin district, northern Iran: Ore-fluid evolution and geodynamic setting. Ore Geol. Rev. 109, 253–275.
Wang, L., Qin, K.Z., Song, G.X., Li, G.M., 2019. A review of intermediate sulfidation epithermal deposits and sub-classification. Ore Geol. Rev. 107, 434–456.
White, N.C., Hedenquist, J.W., 1990. Epithermal environments and styles of mineralization: variations and their causes, and guidelines for exploration. J. Geochem. Explor. 36, 445–474.
Wilkinson, J.J., 2001. Fluid inclusion in hydrothermal ore deposit. Lithos 55, 229–272.
Xie, Y.L., Li, L.M., Wang, B.G., Li, G.M., Liu, H.F., Li, Y.X., Dong, S.L., Zhou, J.J., 2017. Genesis of the Zhaxikang epithermal Pb-Zn-Sb deposit in southern Tibet, China: evidence for a magmatic link. Ore Geol. Rev. 80, 891–909.
Zamanian, H., Rahmani, S.h., Jannesari, M.R., Zareii Sahamieh, R., Borna, B., 2016. Ore genesis study of the Cu-Au vein type deposit in the Tarom granitoid (north Zanjan) based on mineralogical, geochemical and fluid inclusion evidences. Geosciences 98, 255–282 in Persian with English abstract.
Zhu, Y., An, F., Tan, J., 2011. Geochemistry of hydrothermal gold deposits: A review. Geosci. Front. 2, 367–374.